NATIONAL INSTITUTE FOR FUSION SCIENCE

Cross Sections and Oscillator Strengths for Electron-impact
Excitation of Electronic States in Polyatomic Molecules
*-Application Examples of the BEf- scaling model in
Optically-allowed Transitions-*

H. Kato, H. Kawahara, M. Hoshino, M.C. Garcia, S.J. Buckman, M.J. Brunger, L.
Campbell, H. Cho, Y.-K. Kim, J.-S. Yoon, M.-Y. Song, D. Kato, I. Murakami, T. Kato and
H. Tanaka

**RESEARCH REPORT
NIFS-DATA Series**

TOKI, JAPAN

Cross Sections and Oscillator Strengths for Electron-impact Excitation of Electronic States in Polyatomic Molecules

- *Application Examples of the BEf- scaling model in Optically-allowed Transitions*-

H. Kato[1], H. Kawahara[1], M. Hoshino[1], M. C. Garcia[1#], S. J. Buckman[2], M. J. Brunger[3], L. Campbell[3], H. Cho[4], Y.-K. Kim[†], J.-S. Yoon[5], M.-Y. Song[5], D. Kato[6], I. Murakami[6], T. Kato[6], and H. Tanaka[1]

[1]*Department of Physics, Sophia University, Tokyo 102-8554, Japan*
[2]*Center for Antimatter-Matter Studies, Australian National University, Canberra ACT 0200, Australia*
[3]*Center for Antimatter-Matter Studies, Flinders University, GPO Box 2100, Adelaide SA 5001, Australia*
[4]*Department of Physics, Chungnam National University, Daejeon 305-764, Korea*
[5]*Data Center for Plasma Properties, National Fusion Research Institute, 113 Gwahangno, Yuseong-Gu, Daejeon, 305-333, Korea*
[6]*National Institute for Fusion Science, Toki 509-5292, Japan*

1. Introduction
2. Overviews of the theoretical Bethe-Born (BB)-scaling method
   1) Some Consequences of the Born approximation
   2) The Generalized Oscillator Strength (GOS)
   3) The Scaling Methods
   A) Binary-encounter-Bethe (BEB) dipole model
   B) *f*- and *BE*-scaling Models
3. Experimental
   1) Experimental Preliminaries
   2) Fitting procedures of GOS
4. Application examples
   H_2, CO, CO_2, N_2O, H_2O and C_6H_6
5. Concluding Remarks

†Y.-K. Kim deceased (employed at the National Institute of Standards and Technology, 1985-2006, USA, contributed to advances in the Atomic and Molecular Database Project at the National Institute for Fusion Science, particularly during his visit to NIFS in 2001)

#Permanent Address: Ateneo de Zamboanga University, Zamboanga City, Mindanao, Phillipines

Abstract

Integral cross sections for optically allowed electronic-state excitations by electron impact, are reviewed for polyatomic molecules by applying the Binary-Encounter-Bethe (*BEB*) scaling model. Following the context of the present review, the scaling model originally proposed by Yong-Ki Kim to determine electron-impact cross sections for ionization of atoms and molecules is also summarized briefly for its wide range of applications [Electron-Impact Cross Section Database, NIST, Y.-K. Kim][1]. The present report not only focuses on the need for the cross-section data, but also elucidates the verification of the scaling model in the general application for atoms and molecules. Since this report is for a data base, it is summarized for data base users by citing (copying) the descriptions in the original papers and the references within those papers in the style of a textbook.

Keywords: electron scattering, electronic-state excitation, BEf-scaling, cross sections

1. Introduction [2], [3], [4]

A preponderance of matter in the Universe, well over 99%, is in the plasma state, that is, the fourth phase of matter after gases, liquids, and solids. For example, reaction mechanisms in discharge plasmas can be classified into three stages of temporal development, starting with plasma initiation and ending with product formation, which may be designated as "physical", "physicochemical", and "chemical". The physical stage consists of excitation and ionization of atoms and molecules of the reactor gas or gases by electron impact. The physicochemical stage consists of rapid reactions of highly active species, such as slow secondary electrons, positive or negative ions, excited atoms, and radicals resulting from molecular dissociation, with the residual atoms and molecules of the reactor gases, which are mostly in their electronic ground states. The chemical stage consists of thermal reactions of the products of the physicochemical stage with atoms and molecules of the reactor gases. A unifying aspect of complex plasma phenomena

lies in its initiation, which always occurs through collision of energetic electrons with atoms and molecules. Full elucidation of plasma properties must include consideration not only of atomic and molecular processes in the gas phase, but also of the boundary regions, as well as interactions between atoms or molecules with a solid surface, or even with a bulk solid, such as near the reactor wall and the wafer substrate. Thus one can deal with an extremely complex system, containing numerous atomic and molecular species of the reactant gas and solids. However, it is the rich complexity of the system that carries the potential of such diverse phenomena, and hence the possibility of control and design.

Another unifying aspect of the complex plasma phenomena is that ionization is crucial as a source of electrons to maintain the discharges. The kinetic energies of the secondary electrons are mostly ~ 20 eV, nearly independent of the incident electron energy. This fact is reflected in the electron-energy distribution in the bulk plasma.

For electron scattering at incident energies below 1 keV, it is useful to categorize collision phenomena into two classes, depending on a comparison of the momentum of the incident electron relative to that of the "struck" electron initially bound in the target. If the incident electron is fast compared to the orbital velocity of the "struck" electron, one can characterise the process as a fast or non-resonant collision. That is, the incident electron acts only as an impulsive perturbation on the target system. On the other hand, if the incident electron velocity nearly matches the orbital velocities associated with the target electrons, then the collision must be treated differently. In such cases, the incoming slow electron is strongly coupled to the target and becomes indistinguishable from the orbital electrons, at least for some period of time. Thus, the collision complex formed is really more appropriately viewed within the manifold of negative-ion states of the target [see the 2nd NIFS Report]. Another distinction that can be drawn is that fast collisions predominantly involve only small momentum transfer, therefore being governed by the dipole selection rules applicable to photoabsorption. In this third and final report, our intent is to provide a brief guide to the theoretical concepts and formulae necessary for understanding and applying the BEB scaling model, as well as our recent experimental accomplishments for its verification in several molecules.

2. Overview of the theoretical BB-scaling method[1], [4], [5]

In sections 2.1 and 2.2 that follow we have shamelessly borrowed the structure and some content from an earlier review of Celotta and Huebner [4] on electron impact spectroscopy. We gratefully acknowledge here our debt to those authors.

1) *Some Consequences of the Born approximation*

For sufficiently fast electrons, the cross section for a collision that transfers a certain amount of energy and momentum consists of two factors. One factor concerns the kinematics of the scattered electron, and the other describes the excitation properties of the target. In a collision event in which an electron of mass m scatters from a molecule in its ground state and promotes a bound electron to an excited state n with excitation energy E_n, the first Born approximation gives the differential cross section as:

$$\frac{d\sigma}{d\Omega} = 4a_0^2 \frac{k'}{k} K^{-4} |\varepsilon_n(K)|^2, \tag{1}$$

where the interaction potential is taken to be Coulombic and $\boldsymbol{K}$ is the momentum transfer vector, $\boldsymbol{K} = \boldsymbol{k} - \boldsymbol{k}'$. The scalar magnitude of $\boldsymbol{K}$ can be related to the initial and the scattered electron momenta, $\boldsymbol{k}$ and $\boldsymbol{k}'$, and correspondingly to their incident and final energies, T and $T' = T - E_n$, respectively, by conservation of energy and momentum:

$$(Ka_0)^2 = (ka_0)^2 + (k'a_0)^2 - 2kk'a_0^2 \cos\theta \tag{2a}$$

$$= \frac{T}{R} + \frac{T - E_n}{R} - 2\frac{[T(T - E_n)]^{1/2}}{R} \cos\theta, \tag{2b}$$

where T is the reduced kinetic energy; $T = mv^2/2$, a_0 is the Bohr radius (0.529Å), and R is the *Rydberg* energy (13.6eV).

The other quantity in Eq. (1), $|\varepsilon_n(\boldsymbol{K})|$, is the absolute value of the transition matrix element between the initial and final state functions ψ_0 and ψ_n of the target, respectively, given by:

$$\varepsilon_n(\boldsymbol{K}) = \langle \psi_n | \sum_{j=1}^z \exp(i\boldsymbol{K}\cdot\boldsymbol{r}_j) | \psi_0 \rangle, \tag{3}$$

where z is the total number of electrons in the target system, and $\boldsymbol{r}_j$ is the position vector of the j th electron of the target. As mentioned above, Eq. (1) includes two clearly identifiable parts: the first factor is determined completely by the experimental parameters and is simply the Mott cross section for an electron scattered from a free and initially stationary electron. The second factor, referred to as the inelastic-scattering form factor, is a property of the target as is evident from Eq. (3).

2) *The Generalized Oscillator Strength*

In parallel with the theory for the absorption of electromagnetic radiation, Bethe introduced the concept of the *generalized oscillator strength* (GOS) defined by:

$$f_n(K) = E_n / R\,(Ka_0)^{-2}\,|\,\varepsilon_n\,(\boldsymbol{K})\,|^{\,2}. \tag{4}$$

Introducing Eq. (4) into Eq. (1), we obtain an expression for the cross-section:

$$\frac{d\sigma}{d\Omega} = 4a_0^{\,2}\,\frac{k'}{k}\left(\frac{1}{(Ka_0)^2}\right)\frac{f_n(K)}{(E_n/R)} \tag{5a}$$

$$= \frac{4a_0^{\,2}}{T/R}\,\frac{kk'}{K^2}\,\frac{f_n(K)}{(E_n/R)}. \tag{5b}$$

Operationally, one can use Eq. (5) to define an apparent GOS, $f_n\,(K,\,T)$, that is based on the measured cross section and equals *the Bethe GOS* defined by Eqs. (4) and (3) when the Born approximation is valid. The apparent GOS is thus defined by:

$$f_n\,(K,\,T) = \frac{1}{4\pi a_0}\left(\frac{T}{R}\right)\frac{K^2}{kk'}\,\frac{E_n}{R}\,\frac{d\sigma}{d\Omega}, \tag{6a}$$

where:

$$\frac{K^2}{kk'} = \gamma^2 + 4\sin\frac{\theta}{2}, \tag{6b}$$

with:

$$\gamma^2 = \left(1 - \frac{E_n}{T}\right)^{-\frac{1}{2}}\left[1 - \left(1 - \frac{E_n}{T}\right)^{\frac{1}{2}}\right]^2. \tag{6c}$$

All the quantities on the right hand side of Eq. (6) are experimentally observable quantities, and from the experimental point of view Eq. (6) is essentially a definition. Eqs. (3) and (4) then represent only theoretical approximations to this quantity, and should equal

Eq. (6) only for sufficiently large incident electron energies where the Born approximation is valid. It is also important to note that when the Born approximation applies the apparent GOS (Eq. (6a)) is independent of T. Although Eqs. (5a) and (5b) apply to excitations between discrete states, they are readily transformed for transitions to a continuum final state by replacing σ by $d\sigma/dE$ and $f_n(K)$ by $df(K,E)/dE$ as discussed by Inokuti [5]. For such cases $df(K,E)/dE$ is the density of the generalized oscillator strength per unit range of E, and in practice is summed over all discrete and continuum states resulting in an energy transfer at the value E. A formula definition of this density that includes Eq. (4) is:

$$df(K,E)/dE = \sum_n (E_n/R)[|\varepsilon_n(K)|^2/(Ka_0)^2]\delta(E_n - E), \qquad (7)$$

where $\delta(E_n - E)$ is a delta function of the energy transfer. This definition applies equally well for both discrete and continuous energy absorption.

The importance of the GOS formulation introduced by Bethe, arises from the direct relation it bears to the optical (dipole) oscillator strength, f_0, familiar from photoabsorption. This relation is closest in the limit of small momentum transfer, i.e. $K \to 0$ a.u. A straightforward power series expansion of the operator in Eq. (3) gives:

$$\varepsilon_n(K) = \sum_{m=1}^{\infty} \frac{(iKa_0)^m}{m!} \langle \psi_n | \sum_{j=1}^{z} \exp\left(\frac{r_j}{a_0} \cdot \hat{q}\right)^m | \psi_0 \rangle = \sum_{m=1}^{\infty} \frac{(iKa_0)^m}{m!} \varepsilon_{n,m}, \qquad (8)$$

where $\hat{q}$ is a unit vector in the direction of $\mathbf{K}$, $e^{i\mathbf{K}\cdot\mathbf{r}_j} = 1 + i\mathbf{K}\cdot\mathbf{r} + (i)^2/2!(\mathbf{K}\cdot\mathbf{r})^2 +$ higher order terms. Since the GOS is defined in terms of the square of the absolute value of $\varepsilon_n(K)$, clearly only even powers of K occur in a final expression for $f_n(K)$. Using this expansion in Eq. (4), it is easy to show that only the dipole term survives. Consequently,

$$\lim_{K^2 \to 0} f_n(K) = \frac{E_n}{R}|\varepsilon_{n,1}| = f_0 \qquad (9)$$

Although this derivation assumes the same conditions implicit in Eq. (3) (i.e. the Born approximation is physical), it has been shown generally that the limiting value in Eq. (9) is valid regardless of whether the Born approximation holds. This theorem, which we

will refer to as the Lassettre Limit Theorem, appears to be consistent with all the available theoretical and experimental data. It is important to note the following two practical aspects; a) because K=0 a.u. can not be achieved in a real electron collision experiment, the GOS can be determined only at finite values of K and its limiting optical value can only be reached by some extrapolation procedure, b) at low incident electron kinetic energies, the extrapolation may extend over a large region of K and can possibly lead to a large uncertainty in the limiting value obtained. However, due to its generality [6], the limit theorem does provide a sound theoretical basis for comparing electron energy-loss and optical spectra even at impact energies below those considered appropriate for using the Born approximation. This is especially important for the extraction of oscillator strength values from electron-impact measurements.

In terms of the generalized oscillator strength, the integral cross sections can also be obtained as:

$$\sigma(0 \rightarrow n) \ = \ \frac{8\pi a_0}{T_0 / R} \frac{R}{E_n - E_0} \int_{K_{\min}}^{K_{\max}} f_{on}(K) \frac{dK}{K} \qquad (7a)$$

$$= \ \frac{4\pi a_0}{T_0 / R} \frac{R}{E_n - E_0} \int_{K_{\min}}^{K_{\max}} f_{on}(K) d(\ell n K^2), \qquad (7b)$$

where:

$$d\Omega \ = \ sin\theta \ d\theta \ d\varphi \ = \frac{d(K^2)}{2kk'} d\varphi . \qquad (8)$$

Note that $K_{\min}$ and $K_{\max}$ are defined later by Eqs. (19) of this report.

3) *The Scaling Methods*

A theoretical model, which is free of adjustable fitting parameters, for calculating electron-impact cross sections for atoms and molecule is needed in a wide range of applications, such as modeling the plasmas used for plasma processing of semiconductors, designing mercury-free fluorescent lamps, assessing the efficiency of ion gauges, normalizing mass spectrometer output, understanding the plasmas in magnetic fusion devices, and modeling radiation effects on materials. With this aim in mind, Kim and Rudd [7] and Kim [8,9], developed the following scaling methods; the Binary-Encounter-Bethe (*BEB*) dipole, and the scaled first order plane-wave Born – *f*-scaling and *BE*-scaling. These methods are now described in a little more detail.

A. Binary-encounter-Bethe (BEB) dipole model

Combining the Mott cross section with the high-T behavior of the Bethe cross section, an approach, referred to as the *Binary-Encounter-Bethe* (*BEB*) dipole model, is known to be versatile and can successfully provide total and differential ionization cross sections for atoms and molecules [1], [10]. This theory does not use any fitting parameters, and provides a simple analytic formula for the ionization cross section per atomic/molecular orbital. The total ionization cross section for a target is then obtained by summing these cross sections. Four orbital constants – the binding energy B, the orbital kinetic energy U, the electron occupation number N, and a dipole constant Q – are needed for each orbital, and the first three of these are readily available from the ground-state wave function of the target atom or molecule. The basic formula for the ionization cross section per orbital is:

$$\sigma_{BEB} = \frac{S}{t+(u+1)/n}\left[\frac{Q\ell nt}{2}\left(1-\frac{1}{t^2}\right)+(2-Q)\left(1-\frac{1}{t}-\frac{\ell nt}{t+1}\right)\right], \qquad (9)$$

where $t = T/B$, $u = U/B$, $S = 4\pi\, a_0^2 N\, (R/B)^2$, $a_0 = 0.52918\text{Å}$, n is discussed further below shortly and $R = 13.6057$ eV. The dipole constant Q is defined in terms of the continuum dipole oscillator strength df/dW, where W is the kinetic energy of the ionized electron:

$$Q = \frac{2}{N}\int \frac{B}{B+W}\frac{df}{dW}dW\ . \qquad (10)$$

Here, the Mott cross section is defined by generalizing the Rutherford cross section in Eq. (1) for the collision of two electrons, to take account of exchange, as follows:

$$\frac{d\sigma(W,T)}{dW} = \frac{4\pi a_0^2 R^2}{T}\left[\frac{1}{W^2}-\frac{1}{W(T-W)}+\frac{1}{(T-W)^2}\right]. \qquad (11)$$

When df/dW is unknown, one can put $Q = 1$ as a further approximation. The constant n on the right-hand side of Eq. (9) is used for ion targets and for valence orbitals of large atoms, as discussed in more detail in reference [1]. The resulting ionization cross sections for small atoms, a variety of large and small molecules, and radicals are accurate from between 5% to 20%, from threshold to $T \sim 1$ keV, and, is available to the public for a data user through the website [1]. One case of the representative data that illustrates the utility of this approach is shown in Fig. 1 for CF_4. Note that the singly differential

cross section for ejecting an electron with kinetic energy W from an atomic/molecular orbital is also given by the *BEB* model.
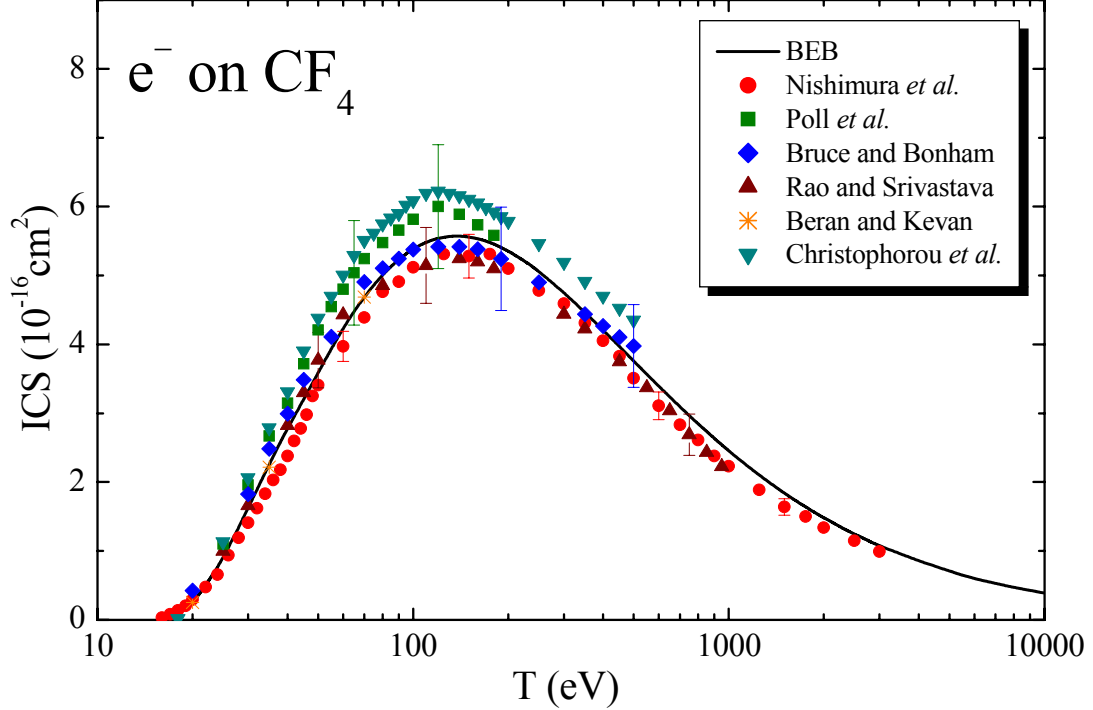

Figure 1 : Total ionization cross section for electron scattering from CF_4. The BEB model result is denoted by the solid line. Data is taken from reference 1.

B. f- and BE-scaling Models

The scaled first order plane-wave Born (PWB) cross sections for integral cross sections of dipole-allowed transitions – *BE*-scaling and *f*-scaling – have been successfully applied for electron-impact excitation of neutral atoms. As the starting point, the PWB is used in the scaling because (a) the plane wave is the correct wave function at infinity for an electron colliding with a neutral atom, and (b) it is the simplest collision theory (i.e. a first-order perturbation theory) that uses the target wave function explicitly in Eq. (7b). Qualitatively, the PWB approximation does not account for the electron exchange effect with the target electrons, the distortion of the plane waves in the vicinity of the target atom, or the polarization of the target due to the presence of the incident electron. It also fails to deal with the types of resonance effects that we discussed in detail in our 2nd NIFS report. These scaling models apply only to integrated excitation cross sections, not to the angular distribution shapes described by the unscaled Born cross sections.

The *f-scaling Born cross section* σ_f is given by:

$$\sigma_f(T) = \frac{f_{accur}}{f_{Born}} \sigma_{Born}(T), \qquad (12)$$

where T is the incident electron energy, f_{accur} is an accurate dipole f value from an accurate wave function or experiment, and f_{Born} is the dipole f value from the same wave function used to calculate the unscaled Born cross section σ_{Born}. The f-scaling process has the effect of replacing the wave function used for σ_{Born} with an accurate wave function.

The *BE- scaled Born cross section* σ_{BE} is given by:

$$\sigma_{BE}(T) = \frac{T}{T + B + E} \sigma_{Born}(T), \qquad (13)$$

where B is the binding energy of the electron being excited and E is the excitation energy. *BE*-scaling corrects the well known deficiency of the Born approximation at low T, without losing its well-known validity at high T.

If we now combine these two models the *BEf - scaled Born cross section* σ_{BEf} is given by:

$$\sigma_{BEf}(T) = \frac{f_{accur}T}{f_{Born}(T + B + E)} \sigma_{Born}(T). \qquad (14)$$

So that if an unscaled σ_{Born} is obtained from poor wave functions while an accurate f value is known, then both f-scaling and *BE*-scaling can be applied to obtain a *BEf*-scaled Born cross section σ_{BEf}.

These three models to scale plane-wave Born cross sections have been shown to produce atomic excitation cross sections comparable in accuracy to those obtained by more sophisticated collision theories, such as the convergent close-coupling (CCC) method, for electron-impact excitation of many neutral atoms. A typical example is shown in Figure 2 for He.
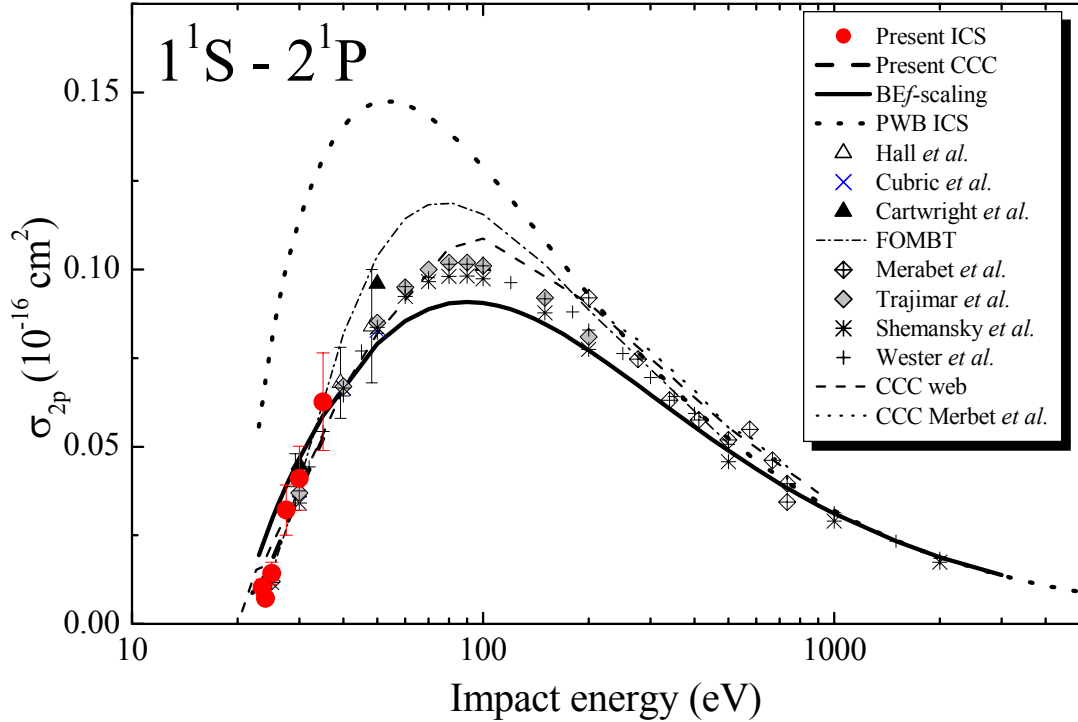
Figure 2 : Electron impact excitation of the 2^1P electronic state in helium. The *BEf*-scaled result is denoted by the solid line. See also the legend on the figure for further details.

We have recently studied in depth [11] excitation of the *n*=2 electronic state manifold in He at the differential cross section level. We found that many of the available data are in good agreement with one another and with sophisticated theories like the CCC approach [11]. Thus, at least for the *n*=2 states, helium can be considered to be a "benchmarked" system. As a consequence, the data shown in Fig. 2 is particularly strong evidence in support of the utility of the scaling methods we have described above.

Just before his tragic death Yong-Ki Kim demonstrated that these models could also be successfully applied to molecular systems and indeed our scaled Born integral cross sections have been found to be in excellent agreement, from near threshold to 200 eV, with those derived from experiments for integral cross sections for electric dipole-allowed transitions in some molecules. In particular we note our results for H_2 [9,12], CO [13,14], CO_2 [15], N_2O [16], H_2O [17] and C_6H_6 as tabulated and plotted later in section 4.

Hence, it has been verified that three quite simple scaling models can convert the PWB for electron-impact excitation of *many* neutral atoms and *molecules* to highly accurate

cross sections at *all incident energies T*, although the original Born cross sections are valid only at high T.

This approach thus shows promise as a universal scaling model for estimating with good accuracy electron impact electronic-state excitation of dipole-allowed transitions and ionization cross sections for a wide range of atoms, molecules and molecular radicals. While it is not capable of dealing with cases where resonance effects are important, it nonetheless represents a relatively straightforward approach by which modelers can extract cross sections of relevance for their application and to use such cross sections with some confidence.

3. Experimental

1) *Experimental Preliminaries*

In our previous two NIFS-DATA reports, we have discussed the apparatus and experimental procedures required to make absolute cross section measurements. We therefore do not repeat those details again here. We do however note that characterizing the analyzer transmission function for the range of scattered electron energies associated with excitation of electronic states in molecules is a challenge. We also highlight that even in simple diatomic molecules there can be significant overlap of vibrational sub-levels of different electronic states, thus complicating the interpretation [18] of the spectra. These are difficult and time-consuming experiments which explains why relatively little work has been undertaken on electronic-state excitation in molecules.

2) *Fitting Procedures of GOS*

An unscaled Born cross section reported in most articles corresponds to the theoretical data in the form of dimensionless GOSs, tabulated as a function of the momentum transfer squared.   As the scaling methods described above are valid only for integral cross sections, it is convenient to present a GOS in an analytical form. Vriens [19] proposed the following formula to represent a GOS for a dipole-allowed excitation:

$$f(x) = \frac{1}{(1+x)^6}\left[\sum_{m=0}^{\infty}\frac{a_m x^m}{(1+x)^m}\right], \qquad (15)$$

where:

$$x = Q/\alpha^2 \qquad (16)$$

and

$$\alpha = \sqrt{B/R} + \sqrt{(B-E)/R} \, . \qquad (17)$$

In Eq. (15), a_m are fitting constants. In the expression α is identified from the analytic properties of the GOS, while the binding energy B of an electron in a many-electron molecule can be defined only in the context of a simple independent particle model. As a fitting parameter along with the a_m, the simple form α^2 in Eq. (16) was found to illustrate a GOS calculated from multiconfiguration wave functions. To fit a theoretical GOS, the optical oscillator strength (OOS) [f_0 in Eq. (15)] should be the one obtained with the same wave functions as those used to calculate the GOS. A GOS for a dipole-allowed excitation usually peaks at the optical limit, i.e., $K = 0$. Sometimes, however, a theoretical GOS has a second peak at a larger K value due to radial nodes in the wave functions.

The same analytic formula can also be used to fit and extrapolate experimental DCS to the forward and backward angles not observed in the experiment, and then to integrate the DCS. Note that here even f_0 should be treated as a fitting parameter. "Experimental" GOS can be obtained by substituting the measured DCSs in Eq. (6a). At low T experimental GOSs often have secondary peaks, as seen in Fig. 3 below. The secondary peaks here have a very different origin than those seen in the theoretical GOS; the former come from interactions not represented in the Born approximation – such as the interference between the direct and exchange scattering amplitudes – while the latter, as noted previously, come from the radial nodes in the wave functions. The secondary peaks in the experimental GOS at low T cannot be well fitted by directly including extra terms in Eq. (15). Instead, the following function with two fitting parameters b and c, in addition to the leading fraction in Eq. (15), was found to represent well the experimental GOS at Low T;

$$g(x) = bx \exp(-cx). \qquad (18)$$
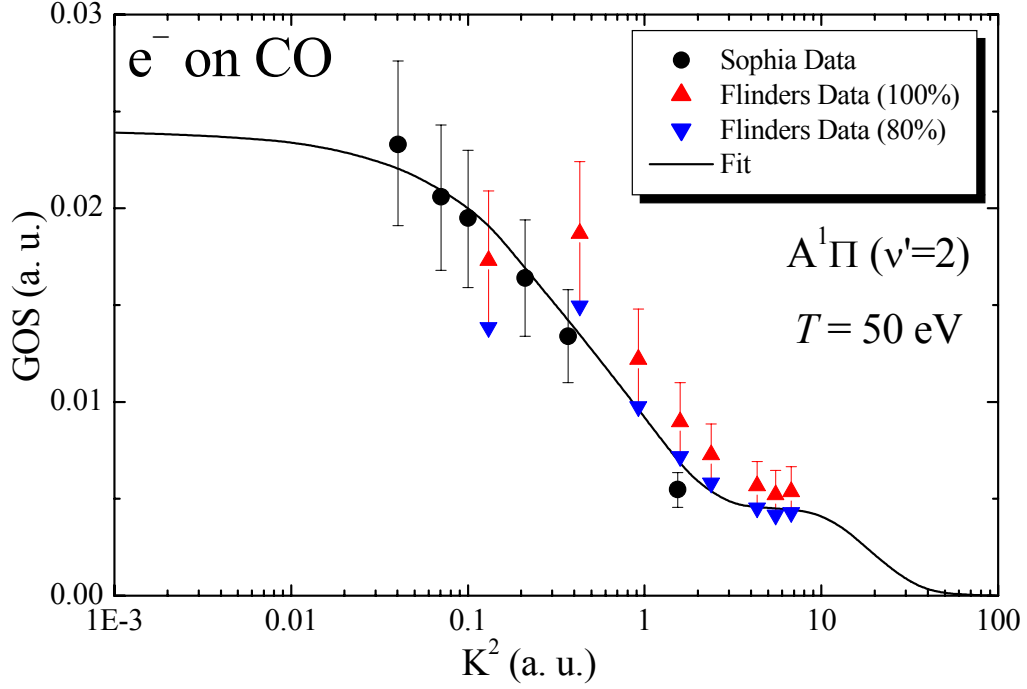
Figure 3 : GOS versus K^2 for electron impact excitation of the $\nu' = 2$ sub-level of the $A^1\Pi$ electronic state in CO. Note the secondary peak at $K^2 \sim 9$ a.u.

Integral cross sections are now obtained by integrating the GOS over the limits corresponding to $\theta = 0°$ and $\theta = 180°$ in Eq. (7a, b) with:

$$K_{\min} = 2\frac{T}{R}\left[1 - \frac{E}{2T} - \sqrt{1 - \frac{E}{T}}\right]$$

and   (19)

$$K_{\max} = 2\frac{T}{R}\left[1 - \frac{E}{2T} + \sqrt{1 - \frac{E}{T}}\right].$$

In the case of the experimental integral cross sections, Eqs. (7a, b) and (19) remain valid, although it is the analytical form of $f_{exp}(K)$ that is explicitly used in Eq. (7a, b), with the result now being the $\sigma_{exp}(T)$ of interest.

4. Application Examples

In this section of our report we now present experimental results and *BEf*-scaling results for the excitation of particular electronic states in the following species:

H_2, CO, CO_2, H_2O, N_2O and C_6H_6.

Given the nature of this report, we do not describe further the cross-section and optical-oscillator / generalized-oscillator strength results we now present. Rather we refer the interested reader to the relevant publications of these data from which full details can be gleaned. Note that most of the data we present was measured at Sophia University, although in some cases supplementary data was also measured at Flinders University.

4.1 H₂

  Full details on the results we present below, for electron impact excitation of some of the electronic states in H_2, can be found in reference [9] (Y.-K. Kim, J. Chem. Phys. <u>126</u> (2007), 064305) and reference [12] (H. Kato, H. Kawahara, M. Hoshino, H. Tanaka, L. Campbell and M. J. Brunger, Phys. Rev. A <u>77</u> (2008), 062708), to whom the interested reader is referred.
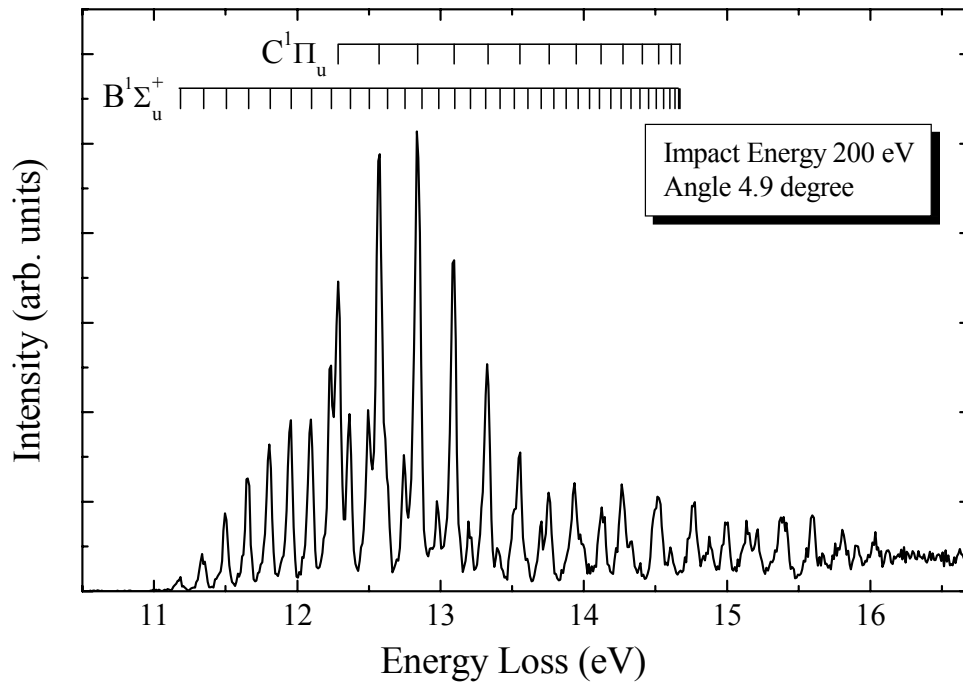
Figure 4.1(a) : Energy loss spectrum of H_2 at an impact energy of 200 eV and for a scattering angle of 4.9 degrees.
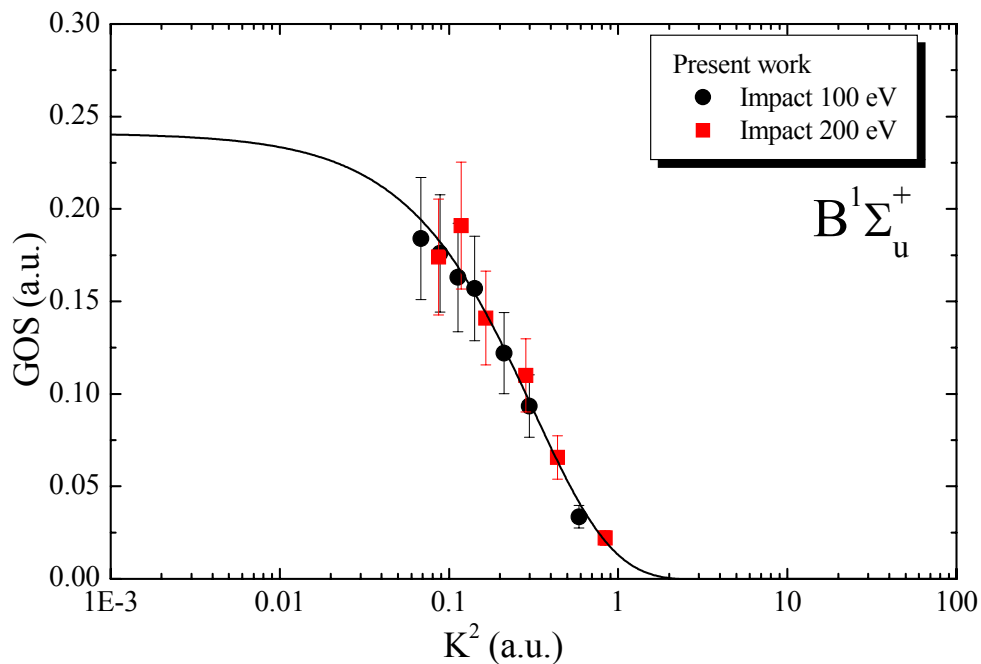
Figure 4.1(b) : GOS as a function of K^2 for the $B^1\Sigma_u^+$ electronic state. This illustrates the procedure for determining the optical oscillator strength (OOS) and the form of the GOS from which the ICS can be determined.

Table 4.1(a). OOSs for the $B^1\Sigma_u^+$ and $C^1\Pi_u$ electronic states.
The error on the present OOSs is ~ 20%.

	$B^1\Sigma_u^+$	$C^1\Pi_u$
Experiment		
Present work	0.241	0.226
Chan *et al.*	0.301	0.322
Xu *et al.*	0.28	0.321
Geiger and Schmoranzer	0.287	0.263
Berkowitz	0.311	0.356
Fabian and Lewis	0.125	0.239
Theory		
Allison and Dalgarno	0.311	0.357
Liu and Hagstrom	0.321	–
Borges and Biel-schowsky	0.274	0.351
Arrighini *et al.*	–	0.349

Figure 4.1(c) : ICSs for the $B^1\Sigma_u^+$ electronic state. See legend on figure for further details.

Figure 4.1(d) : ICSs for the $C^1\Pi_u$ electronic state. See legend on figure for further details.

Table 4.1(b). ICSs for the $B^1\Sigma_u^+$ electronic state. The error on the present ICSs is ~ 25%.

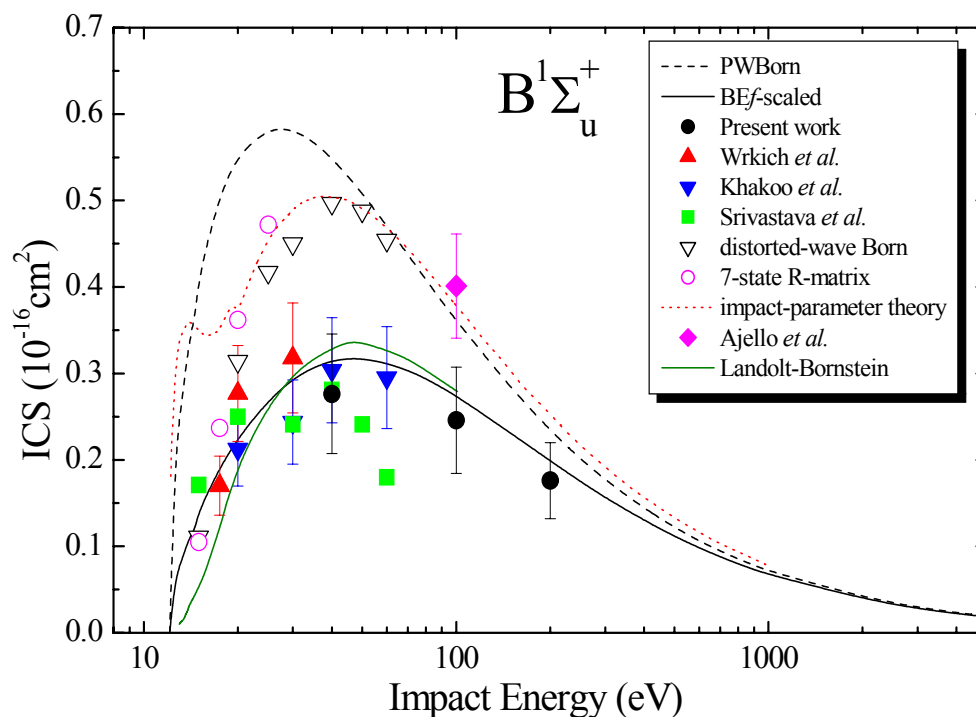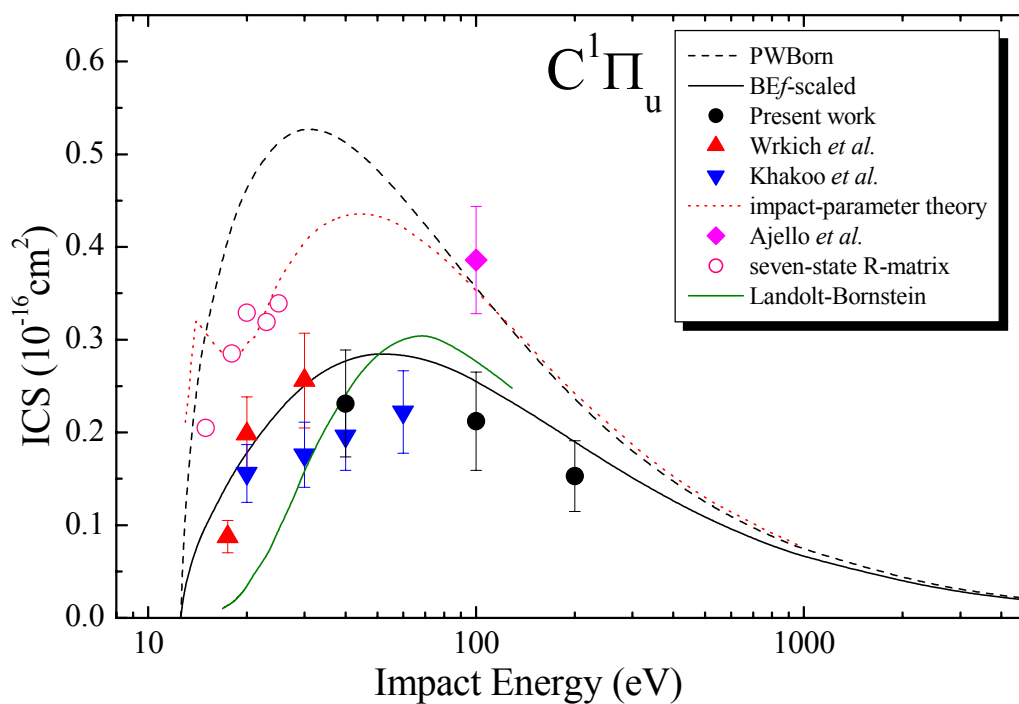| E_0 (eV)	ICS (10^{-16}cm^2)					
	Born	BEf	Present work	Wrkich et $al.$	Khakoo and Trajmar	Srivastava and Jensen
12.1	0.0000	0.0000				
12.571	0.1851	0.0561				
13	0.2514	0.0780				
14.144	0.3499	0.1141				
14.53	0.3607	0.1184				
15	0.4139	0.1412				0.170
17.5	0.5070	0.1905		0.170		
20	0.5529	0.2250		0.277	0.212	0.250
25	0.5845	0.2690				
30	0.5824	0.2937		0.318	0.244	0.240
35	0.5679	0.3074				
40	0.5489	0.3144	0.276		0.304	0.280
45	0.5285	0.3170				
50	0.5083	0.3170				0.240
60	0.4706	0.3119			0.295	0.180
70	0.4379	0.3035				
80	0.4085	0.2939				
90	0.3833	0.2838				
100	0.3612	0.2739	0.246			
150	0.2825	0.2308				
200	0.2340	0.1989	0.176			
250	0.2010	0.1750				
300	0.1768	0.1566				
400	0.1437	0.1300				
500	0.1218	0.1116				
600	0.1062	0.0982				
700	0.0944	0.0878				
800	0.0852	0.0796				
900	0.0777	0.0729				
1000	0.0716	0.0673				
2000	0.0411	0.0392				
3000	0.0295	0.0283				
4000	0.0232	0.0223				
5000	0.0193	0.0185				

Table 4.1(c). ICSs for the $C^1\Pi_u$ electronic state. The error on the present ICSs is ~ 25%.

E_0 (eV)	ICS (10^{-16}cm^2)				
	Born	BEf	Present work	Wrkich *et al.*	Khakoo and Trajmar
12.571	0.0000	0.0000			
13	0.1355	0.0395			
14.144	0.2548	0.0786			
14.53	0.2820	0.0886			
15	0.3106	0.0996			
17.5	0.4127	0.1459		0.088	
20	0.4686	0.1795		0.198	0.156
25	0.5178	0.2245			
30	0.5293	0.2517		0.256	0.176
35	0.5248	0.2680			
40	0.5134	0.2776	0.231		0.196
45	0.4990	0.2828			
50	0.4835	0.2849			
60	0.4527	0.2838			0.222
70	0.4243	0.2786			
80	0.3987	0.2715			
90	0.3760	0.2636			
100	0.3558	0.2555	0.212		
150	0.2820	0.2185			
200	0.2354	0.1898	0.153		
250	0.2032	0.1680			
300	0.1794	0.1509			
400	0.1466	0.1259			
500	0.1247	0.1085			
600	0.1090	0.0957			
700	0.0971	0.0858			
800	0.0877	0.0779			
900	0.0802	0.0715			
1000	0.0739	0.0661			
2000	0.0428	0.0388			
3000	0.0308	0.0280			
4000	0.0243	0.0222			
5000	0.0202	0.0184			

4.2 CO

More information on the results we present below, for electron impact excitation of the $A^1\Pi(v')$, $E^1\Pi$ and $C^1\Sigma^+ + c^3\Pi$ electronic states of CO, can be found in references [13] (H. Kato, H. Kawahara, M. Hoshino, H. Tanaka, M. J. Brunger and Y.-K. Kim, J. Chem. Phys. 126 (2007), 064307) and [14] (H Kawahara, H Kato, M Hoshino H Tanaka and M J Brunger, Phys. Rev. A 77 (2008), 012713). Again the interested reader should consult those papers for further details.
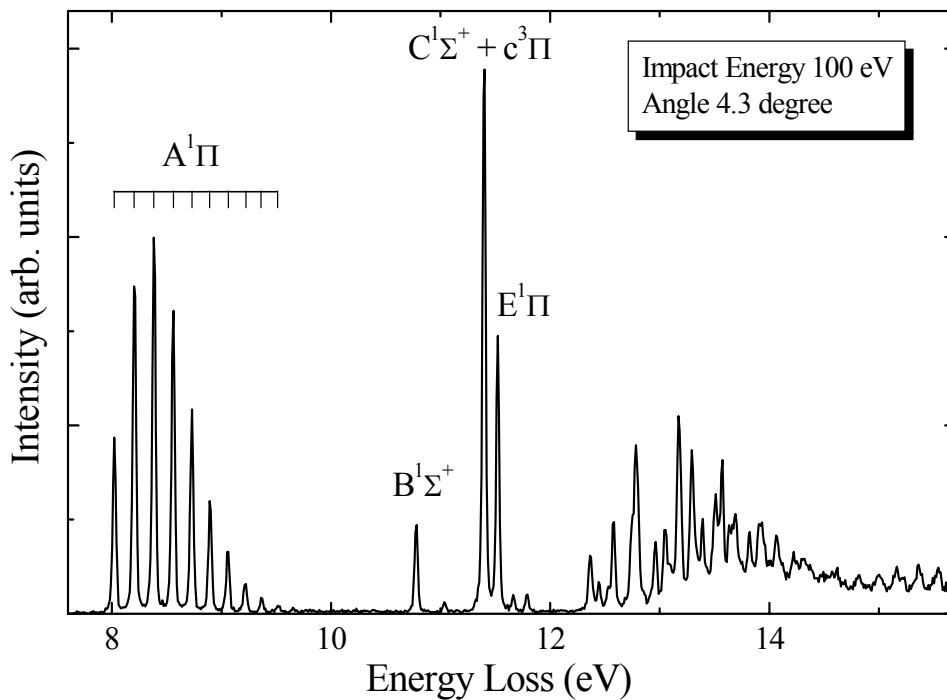

Figure 4.2(a) : Energy loss spectrum of CO at an impact energy of 100 eV and for a scattering angle of 4.3 degrees.
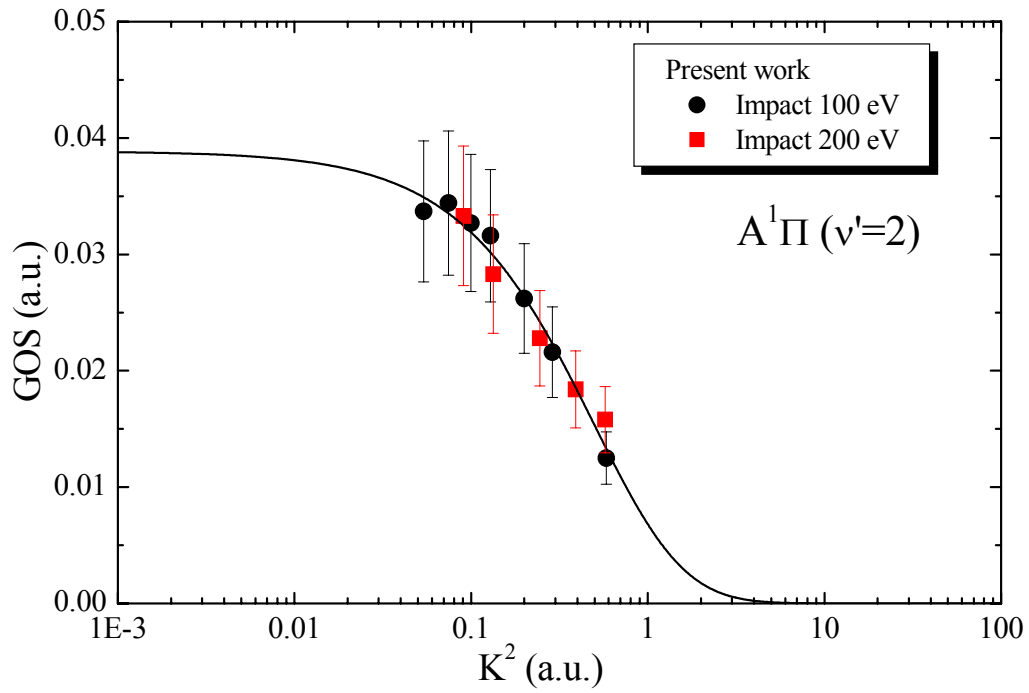
Figure 4.2(b) : GOS versus K^2 for the $A^1\Pi$ (v'=2) electronic state.

Table 4.2(a). OOSs for the A$^1\Pi$, C$^1\Sigma^+$ and E$^1\Pi$ electronic states.
The error on the present OOSs is ~ 20%.

	A$^1\Pi$					
	v'=0	v'=1	v'=2	v'=3	v'=4	v'=5
Experiment						
present work	0.0165	0.0338	0.0389	0.0330	0.0227	0.0136
Chan *et al.*	0.0162	0.0351	0.0402	0.0347	0.0242	0.0145
Zhong *et al.*	0.0166	0.0338	0.0401	0.0325	0.0225	0.0141
Lassettre and Skerble	0.0200	0.0380	0.0429	0.0360	0.0251	0.0155
Eidelsberg *et al.*	0.0165	0.0337	0.0424	0.0377	0.0258	0.0163
Theory						
Chantranupong *et al.*	0.0148	0.0356	0.0473	0.0462	0.0371	0.0262
Kirby and Cooper	0.0155	0.0324	0.0373	0.0316	0.0220	0.0134

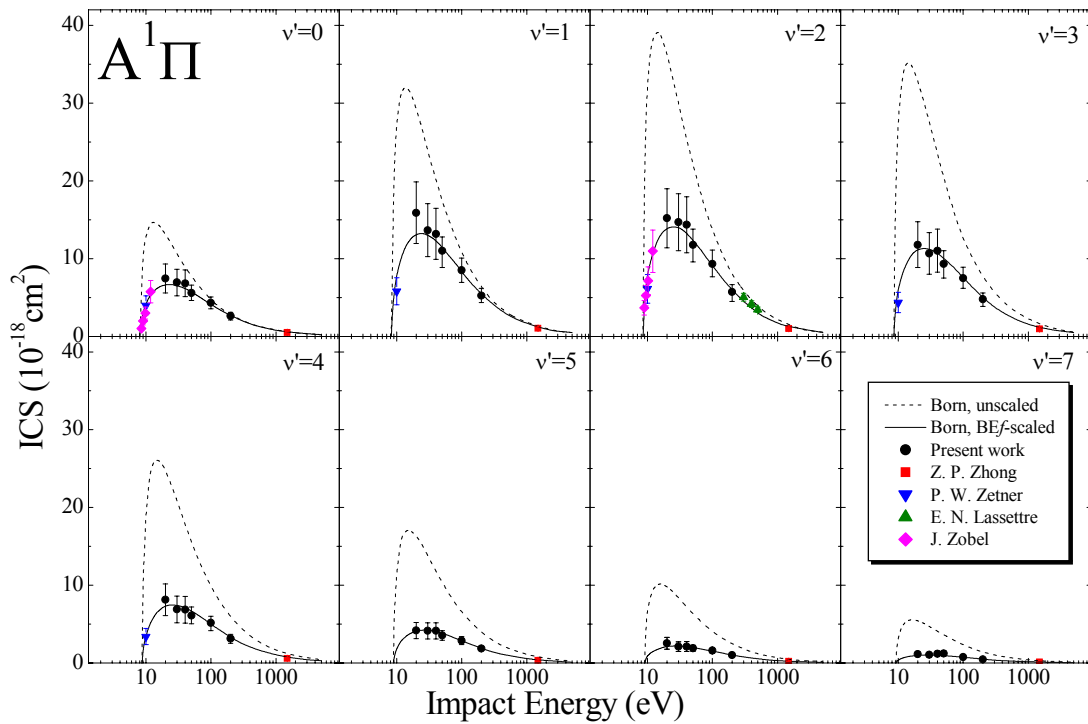|	A$^1\Pi$			C$^1\Sigma^+$	E$^1\Pi$
	v'=6	v'=7	v'=8	v'=0	v'=0
Experiment					
present work	0.00763	0.00377	0.00183	0.1275	0.0640
Chan *et al.*	0.00805	0.00414	0.00202	0.1177	0.0706
Zhong *et al.*	0.0077	0.0043	0.0023	0.1140	0.0642
Lassettre and Skerble	0.00848	0.00437	0.00217	0.163	0.094
Eidelsberg *et al.*	0.0104	0.0059	0.0029	0.0619	0.0365
Theory					
Chantranupong *et al.*	0.0168	0.01	–	0.0647	0.0274
Kirby and Cooper	0.0075	0.0039	0.0019	0.1181	0.049

Figure 4.2(c) : ICSs for the $A^1\Pi$ electronic state. See legend on figure for further details.
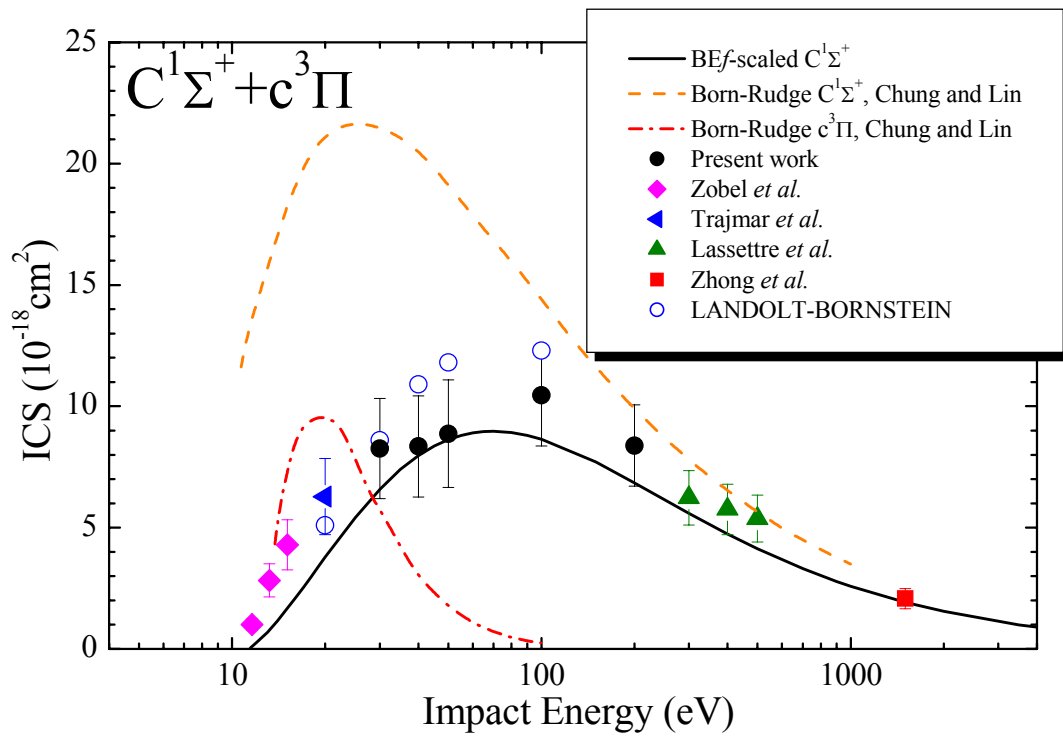

Figure 4.2(d) : ICSs for the $C^1\Sigma^+ + c^3\Pi$ electronic states. See legend on figure for further details.
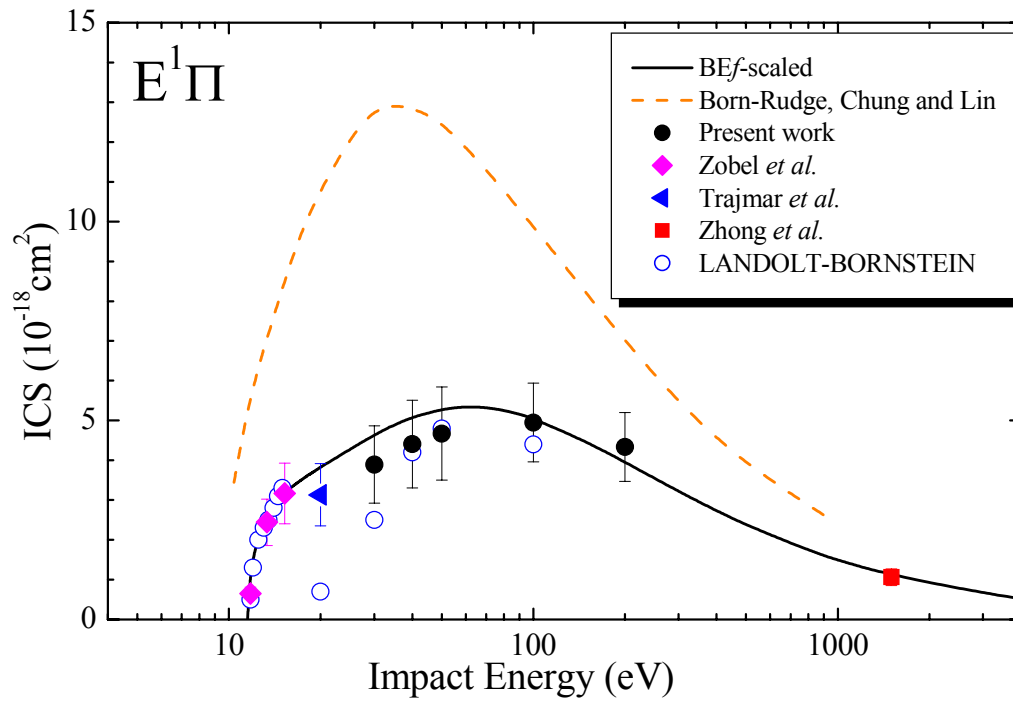
Figure 4.2(e) : ICSs for the $E^1\Pi$ electronic state. See legend on figure for further details.

Table 4.2(b). ICSs for the vibrationally resolved (v'=0 to v'=7) $A^1\Pi$ electronic state. The error on the present ICSs is ~ 30%.

E_0 (eV)	ICS (10^{-18}cm^2)							
	v' = 0		v' = 1		v' = 2		v' = 3	
	BEf	Present work	BEf	Present work	BEf	Present work	BEf	Present work
8.0278	0.000							
8.2115			0.000					
8.3907					0.000			
8.5659							0.000	
9	3.212		5.720		5.338		3.592	
10	4.295		8.097		8.164		6.154	
12	5.438		10.543		10.965		8.564	
14	6.027		11.809		12.412		9.808	
16	6.355		12.531		13.251		10.539	
18	6.538		12.948		13.748		10.983	
20	6.630	7.055	13.176	14.945	14.034	14.421	11.249	11.265
25	6.646		13.289		14.231		11.472	
30	6.514	6.587	13.079	12.808	14.056	13.911	11.375	9.939
35	6.321		12.733		13.720		11.134	
40	6.108	6.811	12.334	13.200	13.317	14.415	10.830	11.044
45	5.891		11.919		12.890		10.502	
50	5.679	5.600	11.508	11.000	12.463	11.800	10.168	9.330
70	4.929		10.035		10.908		8.935	
100	4.098	4.310	8.376	8.510	9.134	9.340	7.507	7.520
200	2.653	2.610	5.454	5.270	5.975	5.720	4.935	4.790
500	1.351		2.792		3.071		2.548	
1000	0.775		1.607		1.772		1.474	
2500	0.360		0.748		0.827		0.689	
5000	0.198		0.412		0.456		0.381	

Table 4.2(b). (continued)

E_0 (eV)	ICS (10^{-18}cm^2)							
	$v' = 4$		$v' = 5$		$v' = 6$		$v' = 7$	
	BEf	Present work	BEf	Present work	BEf	Present work	BEf	Present work
8.7367	0.000							
8.9032			0.000					
9	1.823		0.609					
9.0654					0.000			
9.2234							0.000	
10	3.769		1.938		0.917		0.389	
12	5.462		2.947		1.477		0.673	
14	6.329		3.462		1.760		0.815	
16	6.844		3.771		1.932		0.902	
18	7.162		3.965		2.042		0.960	
20	7.357	7.727	4.080	3.950	2.113	2.443	0.998	1.091
25	7.541		4.218		2.194		1.044	
30	7.502	6.416	4.214	3.883	2.200	1.976	1.053	0.961
35	7.360		4.147		2.172		1.043	
40	7.172	6.831	4.051	4.142	2.126	2.101	1.024	1.189
45	6.964		3.941		2.072		1.000	
50	6.751	6.110	3.827	3.560	2.015	1.890	0.975	1.250
70	5.950		3.388		1.791		0.871	
100	5.013	5.160	2.865	2.890	1.520	1.600	0.742	0.776
200	3.308	3.150	1.908	1.850	1.013	1.010	0.498	0.479
500	1.714		0.989		0.530		0.262	
1000	0.993		0.575		0.308		0.153	
2500	0.465		0.270		0.145		0.072	
5000	0.257		0.150		0.081		0.040	

Table 4.2(c). ICSs for the $C^1\Sigma^+ + c^3\Pi$ electronic states. The error on the present ICSs is ~ 25%. The *BEf*-scaling results only refer to excitation of the $C^1\Sigma^+$ electronic state.

E_0 (eV)	ICS (10^{-18}cm^2)					
	BE*f*	Present work	Zobel *et al.*	Trajmar *et al.*	Lassettre and Skerbele	Zhong *et al.*
11.3965	0.000					
11.5	0.072					
11.6			1.006			
12	0.265					
13	0.689					
13.2			2.825			
14	1.151					
15	1.624					
15.1			4.287			
16	2.092					
17	2.545					
18	2.980					
19	3.394					
20	3.785			6.279		
25	5.412					
30	6.574	8.255				
35	7.394					
40	7.967	8.345				
45	8.364					
50	8.632	8.868				
55	8.806					
60	8.911					
65	8.964					
70	8.978					
80	8.925					
90	8.803					
100	8.643	10.457				
150	7.699					
200	6.846	8.380				
300	5.587				6.229	
400	4.737				5.753	
500	4.127				5.376	
700	3.310					
900	2.783					
1000	2.583					
1500	1.921					2.075
2000	1.545					
3500	0.999					
5000	0.750					

Table 4.2(d). ICSs for the E$^1\Pi$ electronic state. The error on the present ICSs is ~ 25%.

E_0 (eV)	ICS (10^{-18}cm^2)				
	BEf	Present work	Zobel *et al.*	Trajmar *et al.*	Zhong *et al.*
11.5219	0.000				
11.7	0.974				
11.77			0.655		
12	1.539				
13	2.423				
13.32			2.443		
14	2.856				
15	3.126				
15.22			3.169		
16	3.319				
17	3.472				
18	3.603				
19	3.719				
20	3.827			3.131	
25	4.283				
30	4.637	3.892			
35	4.900				
40	5.087	4.409			
45	5.213				
50	5.293	4.673			
55	5.337				
60	5.354				
65	5.351				
70	5.332				
80	5.261				
90	5.164				
100	5.052	4.948			
150	4.464				
200	3.966	4.336			
300	3.234				
400	2.757				
500	2.406				
700	1.969				
900	1.667				
1000	1.553				
1500	1.254				1.060
2000	1.044				
3500	0.575				
5000	0.432				

4.3 CO$_2$

Details on the results presented below, for electron impact excitation of the $^1\Sigma_u^+$ and $^1\Pi_u$ electronic states of CO$_2$, can be found in reference [15] (H. Kawahara, H. Kato, M. Hoshino, H. Tanaka, L. Campbell and M. J. Brunger, J. Phys. B $\underline{41}$ (2008), 085203). Please refer to this paper for further information.
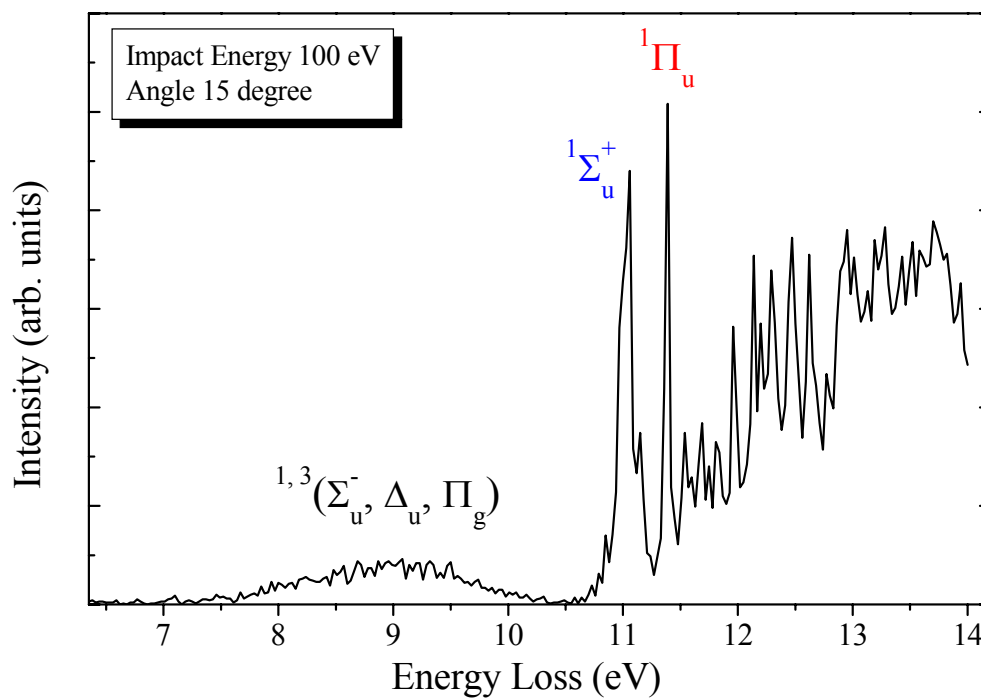

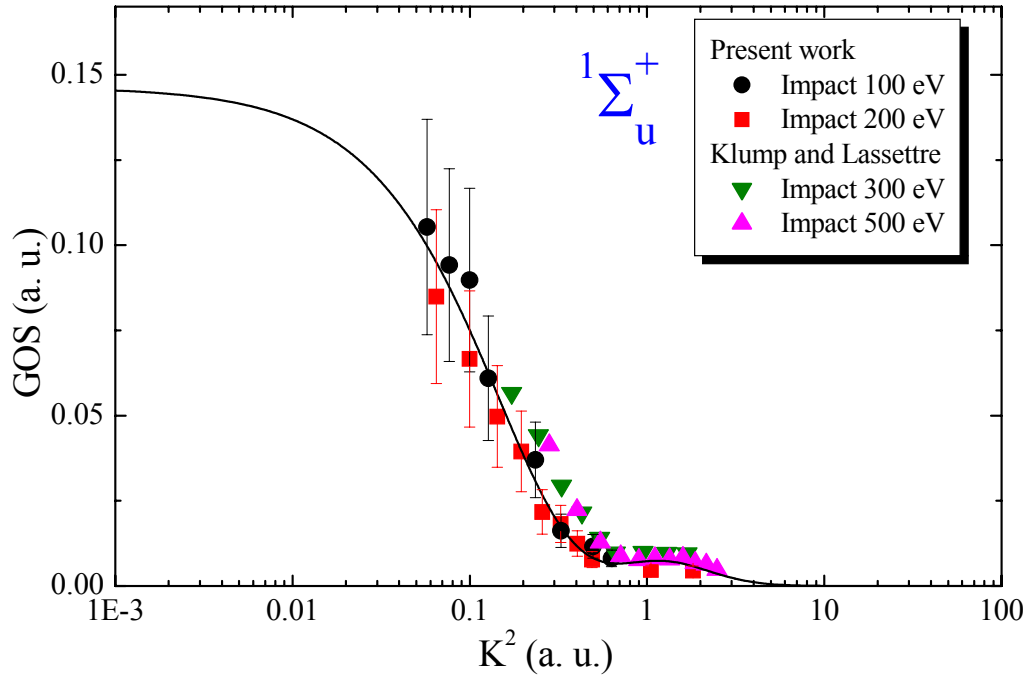Figure 4.3(a) : Energy loss spectrum of CO$_2$ at an impact energy of 100 eV and for a scattering angle of 15 degrees.

Figure 4.3(b) : GOS versus K^2 for the $^1\Sigma_u^+$ electronic state. See legend on figure for further details.

Table 4.3(a). OOSs for the $^1\Sigma_u^+$ and $^1\Pi_u$ electronic states. The error on the present OOSs is ~ 30%.

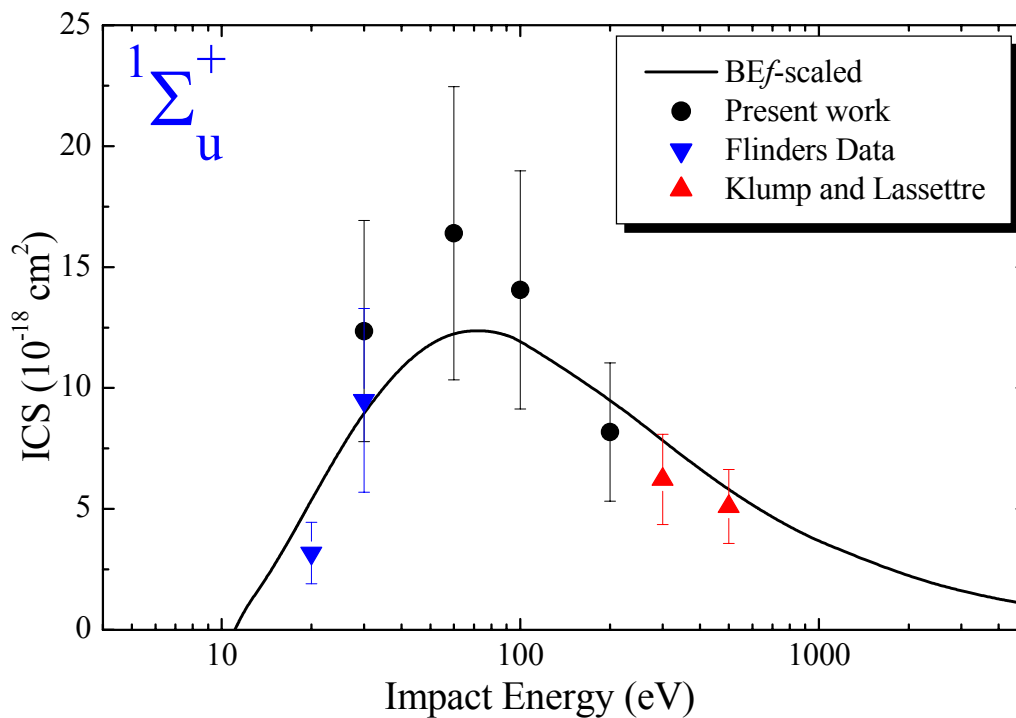|	$^1\Sigma_u^+$	$^1\Pi_u$
Experiment		
present work	0.147	0.057
W. F. Chan *et al.*	0.171	0.060
Klump and Lassettre	0.119	0.045
Inn *et al.*	0.120	–
Theory		
Buenker *et al.*	0.085	0.048
McCurdy and McKoy	0.116	0.116
Padial *et al.*	0.046	0.030

Figure 4.3(c) : ICSs for the $^1\Sigma_u^+$ electronic state. See legend on figure for further de-
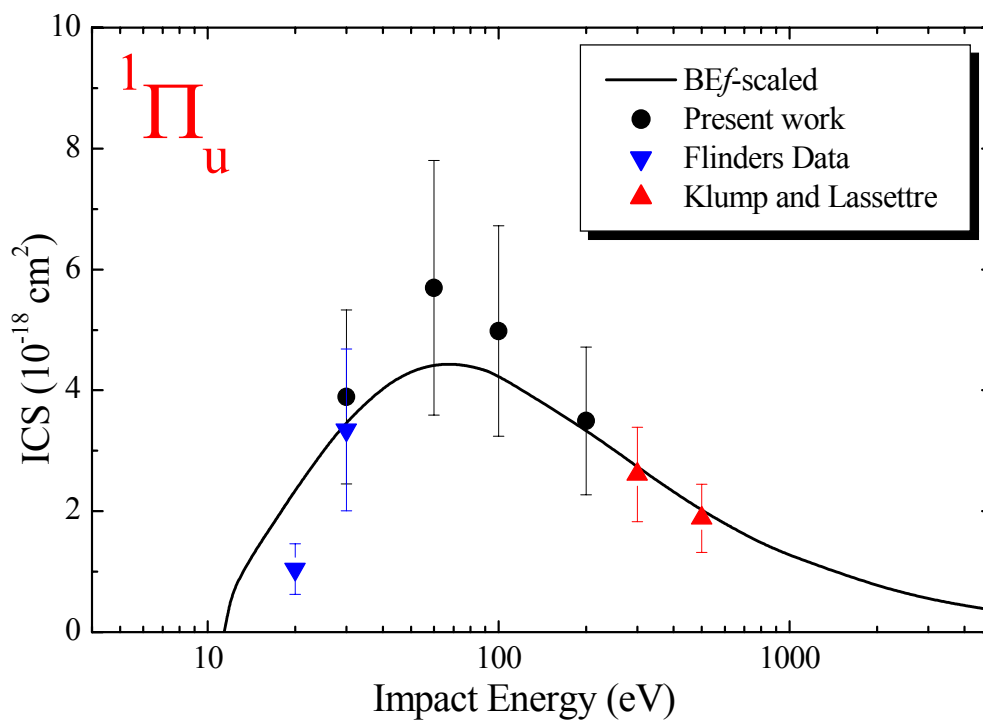tails.

Figure 4.3(d) : ICSs for the $^1\Pi_u$ electronic state. See legend on figure for further details.

Table 4.3(b). ICSs for the $^1\Sigma_u^+$ electronic state. The error on the present ICSs is ~ 37%.

| E_0 (eV) | ICS (10^{-18}cm^2) | | | |
	BEf	Present work	Flinders	Klump and Lassettre
11.048	0.000			
12	0.877			
13	1.484			
14	2.081			
15	2.673			
16	3.254			
17	3.818			
18	4.362			
19	4.883			
20	5.379		3.175	
25	7.483			
30	9.026	12.352	9.490	
40	10.926			
50	11.863			
60	12.275	16.398		
70	12.393			
80	12.342			
90	12.193			
100	11.977	14.058		
200	9.555	8.177		
300	7.824			6.221
400	6.647			
500	5.800			5.097
600	5.161			
700	4.660			
800	4.256			
1000	3.643			
2000	2.186			
3000	1.598			
4000	1.273			
5000	1.064			

Table 4.3(c). ICSs for the $^1\Pi_u$ electronic state. The error on the present ICSs is $\sim 37\%$.

E_0 (eV)	ICS (10^{-18}cm^2)			
	BEf	Present work	Flinders	Klump and Lassettre
11.385	0.000			
12	0.580			
13	0.939			
14	1.204			
15	1.432			
16	1.640			
17	1.834			
18	2.014			
19	2.184			
20	2.344		1.043	
25	3.007			
30	3.483	3.892	3.345	
40	4.056			
50	4.324			
60	4.428	5.696		
70	4.440			
80	4.401			
90	4.333			
100	4.245	4.982		
200	3.349	3.493		
300	2.732			2.608
400	2.317			
500	2.019			1.883
600	1.795			
700	1.619			
800	1.478			
1000	1.264			
2000	0.757			
3000	0.553			
4000	0.440			
5000	0.368			

4.4 H$_2$O

Further information on the figures and tables given below, for excitation by electrons of the A^{1}B$_1$ electronic state in H$_2$O, can be found in reference [17] (P. A. Thorn, M. J. Brunger, P. J. O. Teubner, N. Diakomichalis, T. Maddern, M. A. Bolorizadeh, W. R. Newell, H. Kato, M. Hoshino, H. Tanaka, H. Cho and Y.-K. Kim, J. Chem. Phys. 126 (2007), 064306). The reader is again asked to consult this paper if more detail is required.
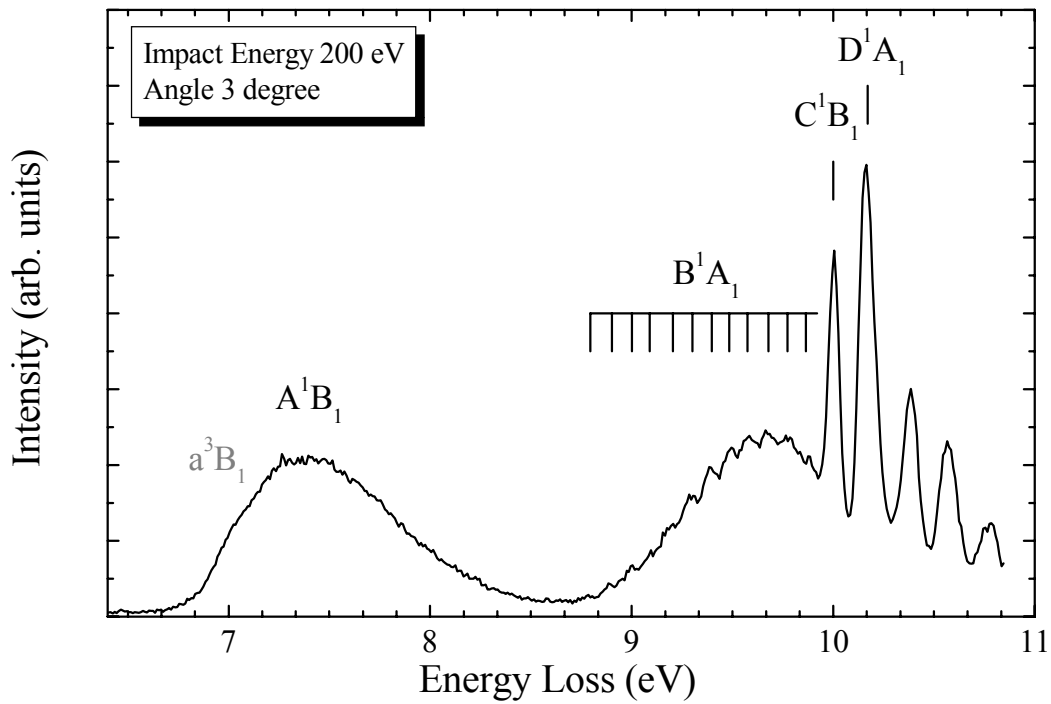

Figure 4.4(a) :   Energy loss spectrum of H$_2$O at an impact energy of 200 eV and for a scattering angle of 3 degrees.
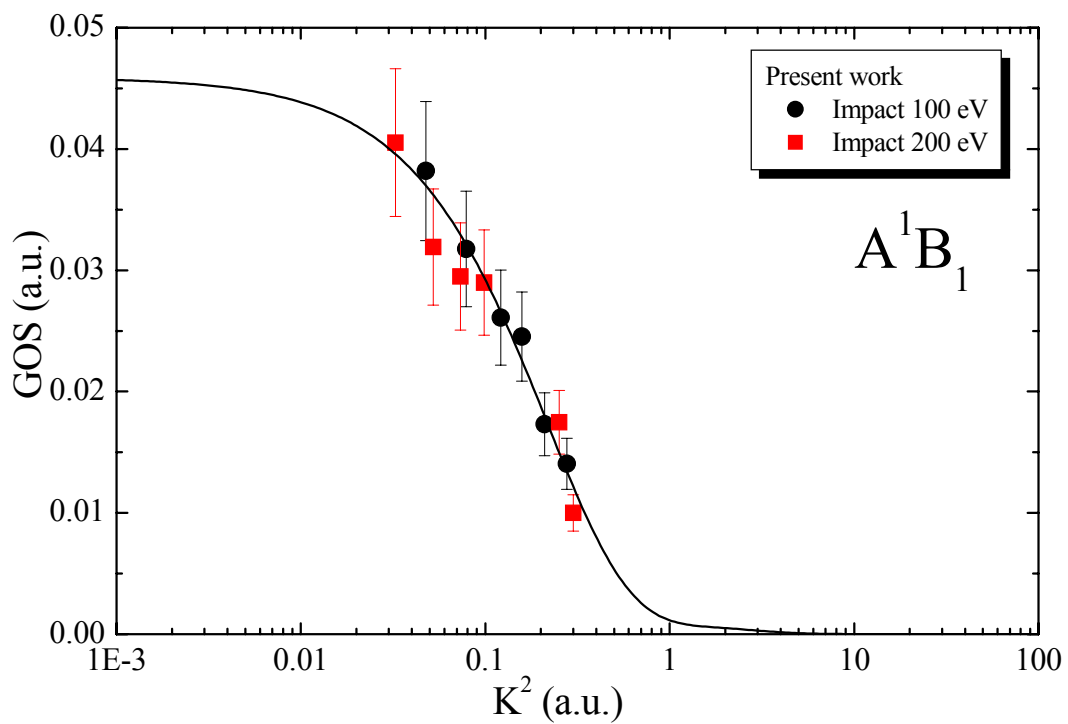
Figure 4.4(b) : GOS versus K^2 for the A^{1}B$_1$ electronic state.

Table 4.4(a). OOSs for the A^1B_1 electronic state.

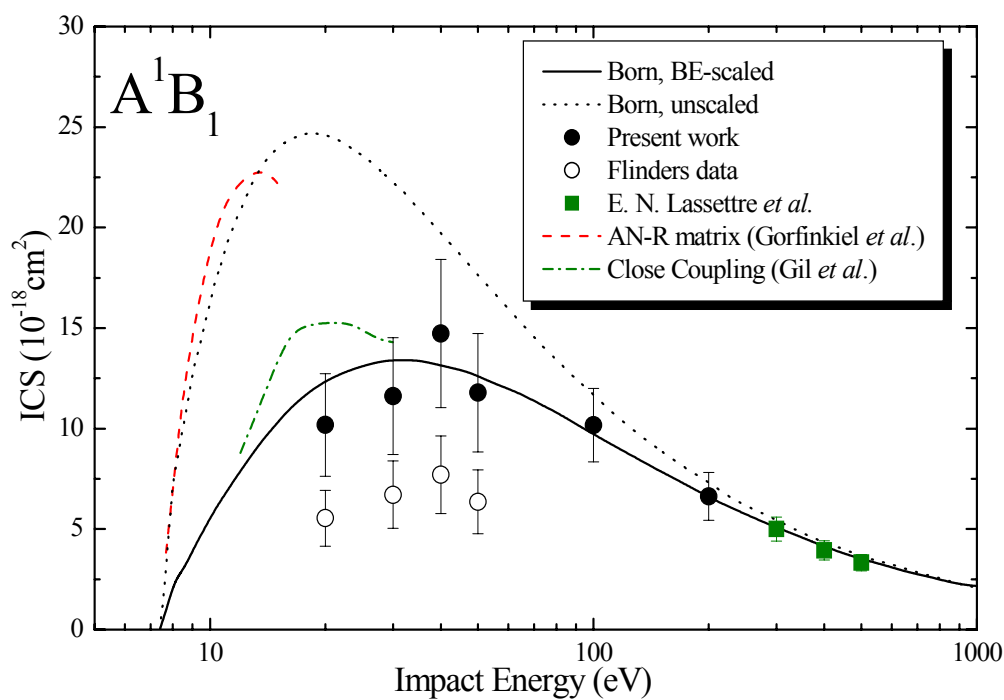|	f_l	f	f_v
Experiment			
Present work		0.0459 ± 0.0069	
Yoshino *et al.*		0.046	
Chan *et al.*		0.0497	
Lee and Suto		0.0456	
Lassettre and White		0.060	
Laufer and McNesby		0.041	
Theory			
Phillip and Buenker	0.0500		0.0576
Bhanuprakash *et al.*		0.054	
Durante *et al.*		0.046	
Theodorakopoulos *et al.*		0.065	
Diercksen *et al.*	0.0208		
Williams and Langhoff	0.0360		
Buenker and Peyerimhoff	0.0592		0.0779
Wood	0.0370		

Figure 4.4(c) : ICSs for the A^1B_1 electronic state. See legend on figure for further details.

Table 4.4(b). ICSs for the A^1B_1 electronic state. The error on the present ICSs is ~ 31%.

E_0 (eV)	ICS (10^{-17}cm^2)				
	Born	BE	Present work	MPSA (Flinders)	Lassettre
10	1.6380	0.5457			
15	2.3653	1.0260			
20	2.4596	1.2293	1.018	0.554	
25	2.3603	1.3108			
30	2.2270	1.3357	1.162	0.671	
35	2.0945	1.3324			
40	1.9721	1.3143	1.473	0.770	
45	1.8617	1.2885			
50	1.7627	1.2588	1.178	0.635	
55	1.6740	1.2273			
60	1.5943	1.1954			
70	1.4571	1.1331			
80	1.3435	1.0746			
90	1.2479	1.0209			
100	1.1663	0.9718	1.017		
200	0.7249	0.6590	0.663		
300	0.5385	0.5048			0.0507
400	0.4332	0.4126			0.0399
500	0.3648	0.3507			0.0334
600	0.3164	0.3062			
700	0.2802	0.2724			
800	0.2520	0.2458			
900	0.2293	0.2243			
1000	0.2107	0.2065			
2000	0.1195	0.1183			
3000	0.0851	0.0846			
4000	0.0668	0.0665			
5000	0.0553	0.0550			

4.5 N$_2$O

Full details on the results presented below, for electron impact excitation of the C$^1\Pi$ and D$^1\Sigma^+$ electronic states in N$_2$O, can be found in reference [16] (H. Kawahara, D. Suzuki, H. Kato, M. Hoshino, H. Tanaka, O. Ingolfsson, L. Campbell and M. J. Brunger, J. Chem. Phys. <u>131</u> (2009), 114307). Again, the interested reader should consult that paper for further information.
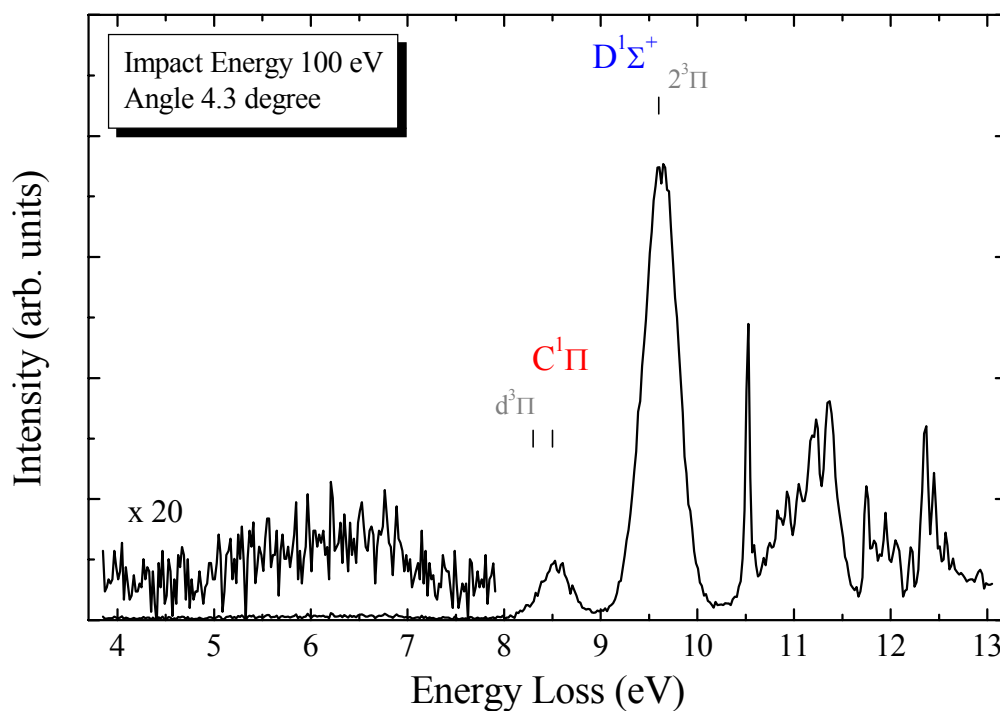

Figure 4.5(a) : Energy loss spectrum of N$_2$O at an impact energy of 100 eV and for a scattering angle of 4.3 degrees.
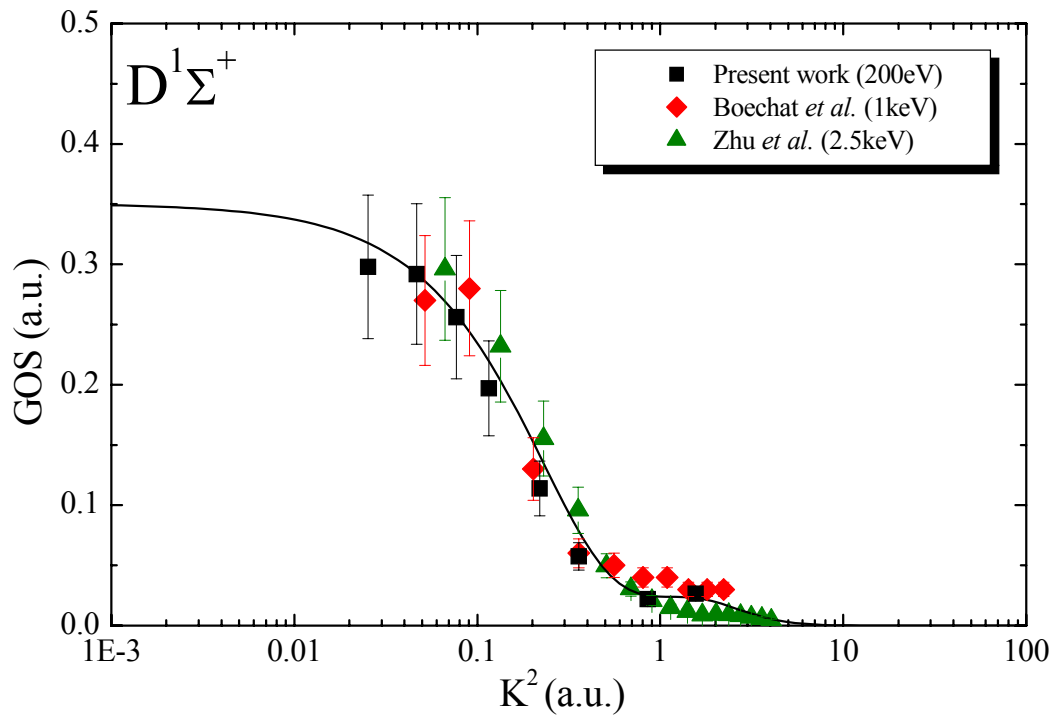
Figure 4.5(b) : GOS versus K^2 for the D$^1\Sigma^+$ electronic state. See legend on figure for
further details.

Table 4.5(a). OOSs for the C$^1\Pi$ and D$^1\Sigma^+$ electronic states.
The error on the present OOSs is ~ 21%.

	C$^1\Pi$	D$^1\Sigma^+$
Experiment		
present work	0.0233	0.350
W. F. Chan *et al.*	0.0245	0.376
Lee and Suto	0.0253	0.378
Huebner *et al*.	0.0285	0.352
Rabalais *et al*.	0.007	0.36
Zelikoff *et al*.	0.0211	0.367
Theory		
Chutjian and Segal	0.029	0.77
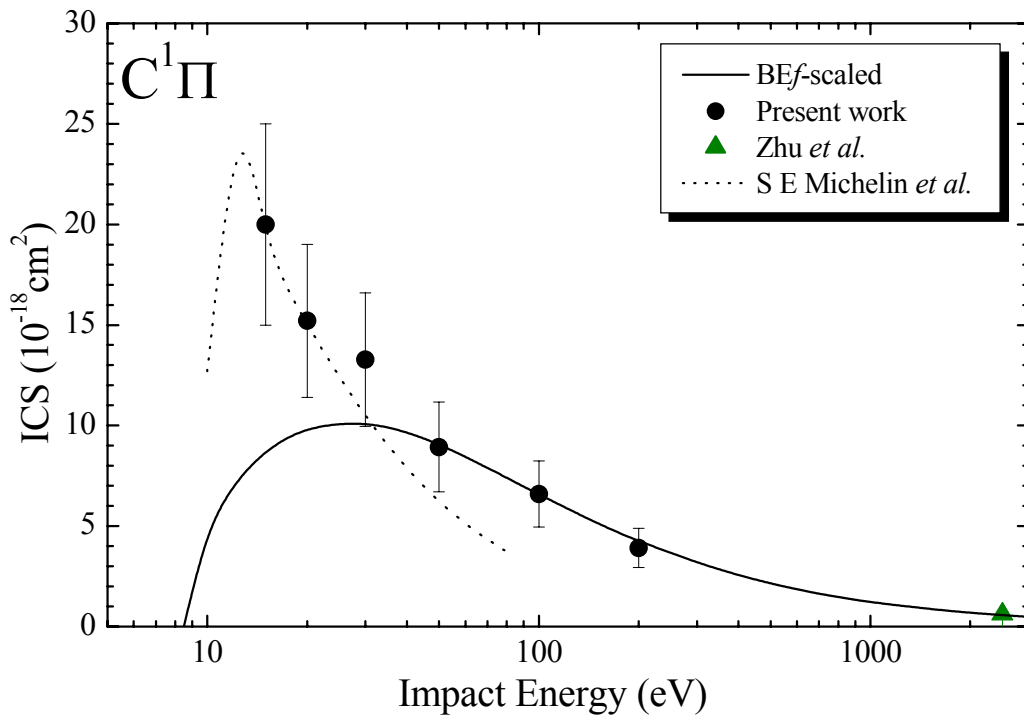
Figure 4.5(c) : ICSs for the C$^1\Pi$ electronic state. See legend on figure for further details.
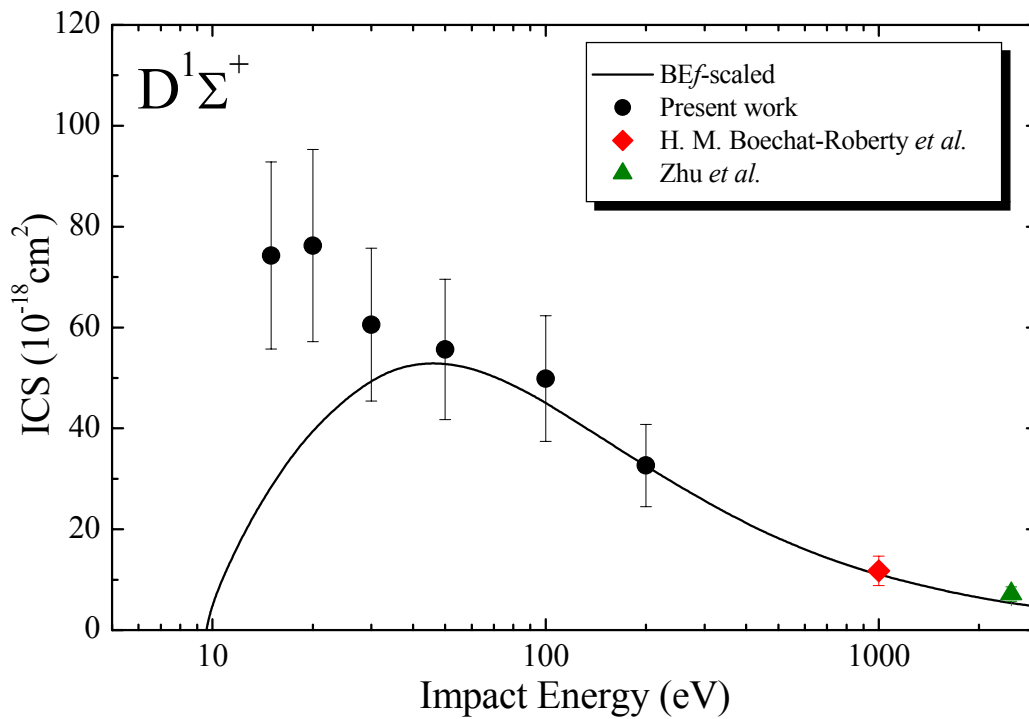

Figure 4.5(d) : ICSs for the D$^1\Sigma^+$ electronic state. See legend on figure for further details.

Table 4.5(b). ICSs for the $C^1\Pi$ electronic state. The error on the present ICSs is $\sim 25\%$.

E_0 (eV)	ICS (10^{-18}cm^2)		
	BEf	Present work	Zhu $et\ al.$
8.5	0.00		
10	4.85		
12	7.09		
15	8.82	19.99	
20	9.97	15.21	
30	10.20	13.28	
40	9.69		
50	9.06	8.93	
60	8.45		
70	7.89		
80	7.40		
90	6.96		
100	6.57	6.60	
150	5.14		
200	4.24	3.91	
300	3.17		
400	2.55		
500	2.14		
600	1.86		
700	1.64		
800	1.47		
900	1.34		
1000	1.23		
1500	0.87		
2000	0.68		
2500	0.57		0.62
3000	0.48		
4000	0.38		
5000	0.31		

Table 4.5(c). ICSs for the $D^1\Sigma^+$ electronic state. The error on the present ICSs is ~ 25%.

E_0 (eV)	BEf	ICS (10^{-18}cm^2)		
		Present work	Boechat-Roberty et al.	Zhu et al.
9.6	0.00			
10	5.78			
12	17.43			
15	28.82	73.42		
20	40.27	76.24		
30	50.17	60.57		
40	52.94			
50	52.98	55.64		
60	51.87			
70	50.30			
80	48.56			
90	46.80			
100	45.08	49.87		
150	37.79			
200	32.49	32.64		
300	25.53			
400	21.18			
500	18.18			
600	15.99			
700	14.31			
800	12.97			
900	11.88			
1000	10.98		11.75	
1500	8.04			
2000	6.40			
2500	5.35			7.16
3000	4.62			
4000	3.65			
5000	3.03			

4.6 C_6H_6

Work on electron impact excitation of the $^1B_{1u}$ and $^1E_{1u}$ electronic states in benzene is currently in progress. Preliminary results were presented recently at the 16th International Symposium on Electron-Molecule Collisions and Swarms in Toronto, Canada. We therefore reproduce some of these data, at 100 eV and 200 eV, which also strongly suggests that the scaling models we have described can be applied to larger molecular systems.
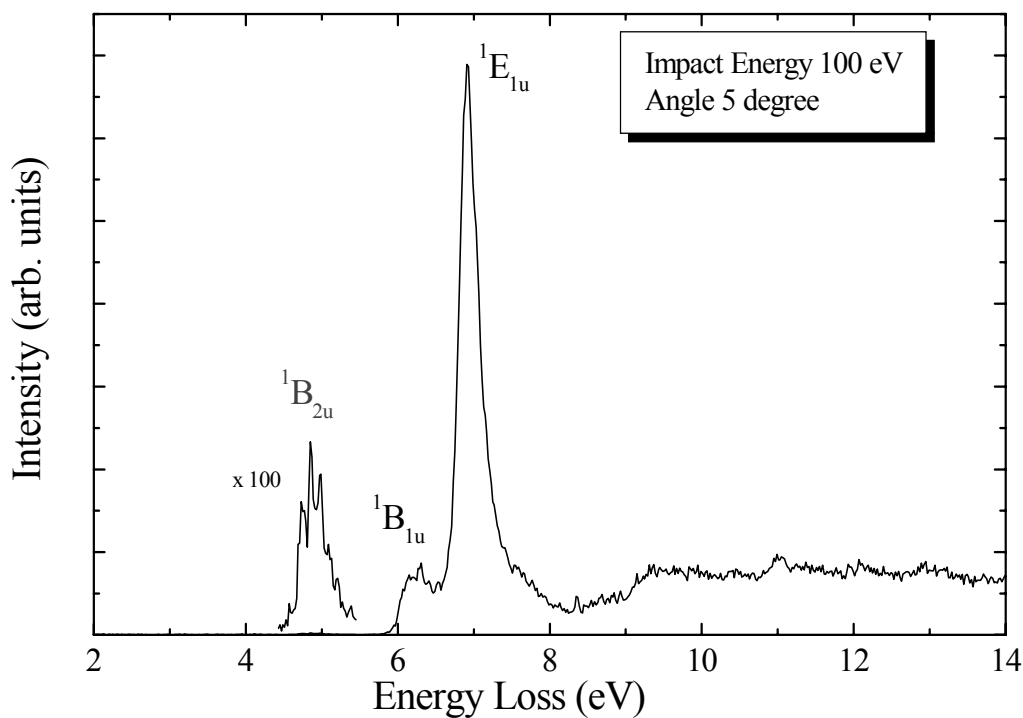

Figure 4.6(a) : Energy loss spectrum of C_6H_6 at an impact energy of 100 eV and for a scattering angle of 5 degrees.
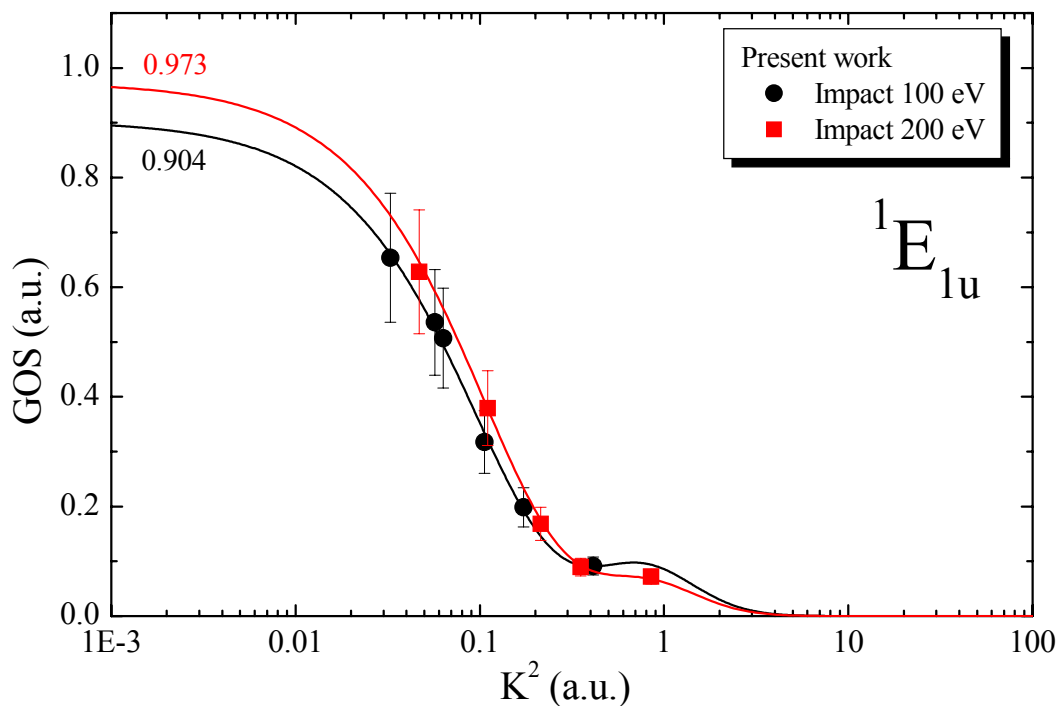
Figure 4.6(b) : GOS versus K^2 for the $^1E_{1u}$ electronic state.

Table 4.6(a). OOSs for the $^1B_{1u}$ and $^1E_{1u}$ electronic states.

	State (energy at the continuum maximum)	
	$^1B_{1u}$ (6.19 eV)	$^1E_{1u}$ (6.96 eV)
Experiment		
Present work	0.110 ± 0.025	0.953 ± 0.172
Hammond and Price	0.094	0.88
Pantos *et al*.	0.090	0.953
Philis *et al*.	0.090	0.900
Suto *et al*.	0.03	0.84
Feng *et al*.	0.031	0.824
Boechat *et al*.	0.094	0.88
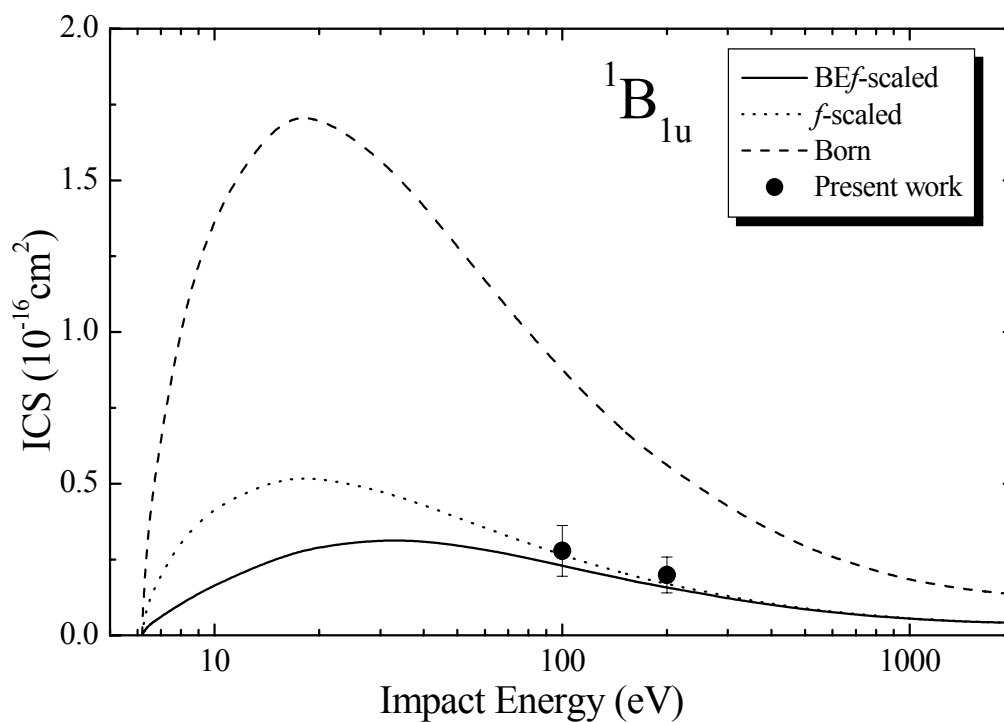
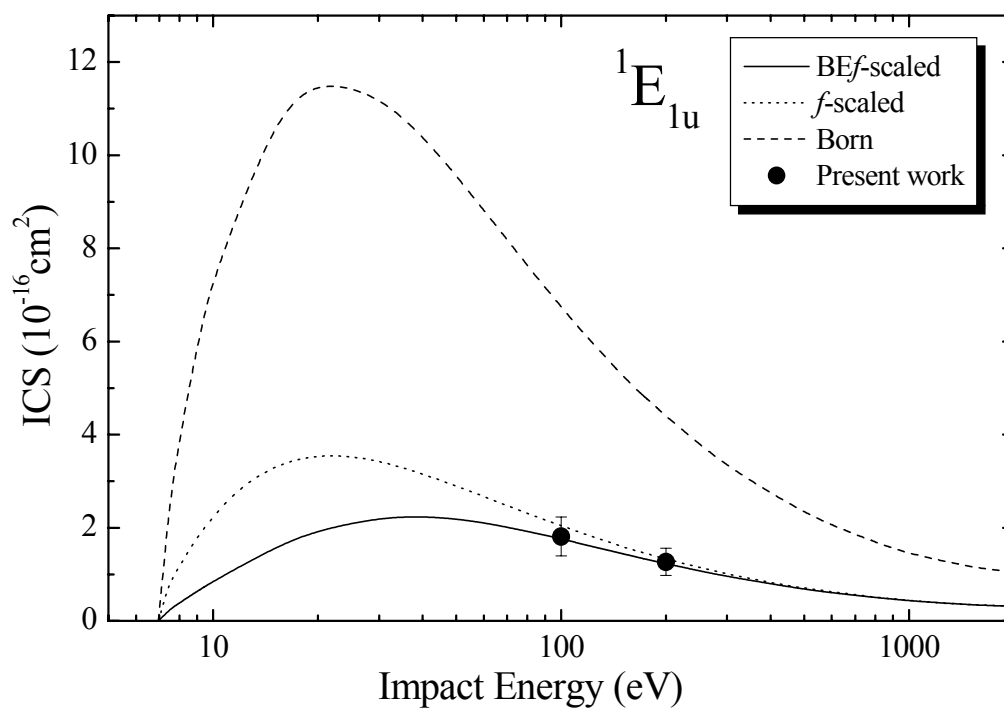Figure 4.6(c) : ICSs for the $^1B_{1u}$ electronic state.

Figure 4.6(d) : ICSs for the $^1E_{1u}$ electronic state.

Table 4.6(b). ICSs for the $^1B_{1u}$ electronic state. The error on the present ICSs is $\sim$ 30%.

E_0 (eV)	ICS (10^{-16}cm^2)			
	Born	f-scaled	BEf	Present work
6.19	0.0000	0.0000	0.0000	
6.4	0.3107	0.0941	0.0276	
6.6	0.4458	0.1351	0.0405	
7	0.6496	0.1969	0.0614	
7.5	0.8459	0.2563	0.0838	
8	1.0025	0.3038	0.1037	
8.5	1.1305	0.3426	0.1217	
9	1.2363	0.3746	0.1380	
9.5	1.3243	0.4013	0.1529	
10	1.3978	0.4236	0.1666	
15	1.7066	0.5172	0.2549	
20	1.7185	0.5208	0.2940	
30	1.5754	0.4774	0.3153	
40	1.4170	0.4294	0.3099	
50	1.2819	0.3885	0.2969	
60	1.1703	0.3546	0.2821	
70	1.0775	0.3265	0.2676	
80	0.9995	0.3029	0.2539	
90	0.9331	0.2828	0.2414	
100	0.8758	0.2654	0.2299	0.279
150	0.6770	0.2052	0.1860	
200	0.5601	0.1697	0.1576	0.199
300	0.4216	0.1278	0.1215	
400	0.3448	0.1045	0.1006	
500	0.2928	0.0887	0.0861	
600	0.2585	0.0783	0.0764	
700	0.2336	0.0708	0.0693	
800	0.2120	0.0642	0.0630	
900	0.1975	0.0599	0.0589	
1000	0.1833	0.0555	0.0547	
1500	0.1483	0.0449	0.0445	
2000	0.1361	0.0412	0.0409	

Table 4.6(c). ICSs for the $^1E_{1u}$ electronic state. The error on the present ICSs is ~ 23%.

E_0 (eV)	ICS (10^{-16}cm^2)			
	Born	f-scaled	BEf	Present work
6.96	0.0000	0.0000	0.0000	
7.5	2.5932	0.7858	0.2487	
8	3.8748	1.1742	0.3882	
8.5	4.9424	1.4977	0.5154	
9	5.8587	1.7754	0.6341	
9.5	6.6522	2.0158	0.7451	
10	7.3419	2.2248	0.8492	
15	10.8507	3.2881	1.5808	
20	11.6534	3.5313	1.9510	
30	11.2839	3.4194	2.2204	
40	10.4115	3.1550	2.2456	
50	9.5641	2.8982	2.1890	
60	8.8218	2.6733	2.1049	
70	8.1844	2.4801	2.0140	
80	7.6365	2.3141	1.9244	
90	7.1625	2.1704	1.8394	
100	6.7489	2.0451	1.7600	1.812
150	5.2822	1.6007	1.4447	
200	4.3982	1.3328	1.2329	1.269
300	3.3365	1.0111	0.9593	
400	2.7374	0.8295	0.7972	
500	2.3308	0.7063	0.6841	
600	2.0576	0.6235	0.6071	
700	1.8566	0.5626	0.5499	
800	1.6852	0.5107	0.5005	
900	1.5661	0.4746	0.4662	
1000	1.4523	0.4401	0.4331	
1500	1.1551	0.3500	0.3463	
2000	1.0363	0.3140	0.3115	
3000	1.0047	0.3045	0.3028	

5. Concluding Remarks

We have reported on some relatively straightforward models for calculating ionization cross sections and dipole-allowed electronic-state excitation cross sections for atomic and molecular systems, including for molecular radicals. These approaches seem to have real utility in providing accurate (to ~ 20% level in many cases) cross section data for workers seeking to model the behavior of applications including low-temperature plasma reactors and fusion reactors. In support of our arguments we have also presented results from six molecular systems, for optical oscillator strengths and integral cross sections of a subset of those molecules' electronic states. The present report, the third and final in our NIFS Data Series, would not have been possible without the seminal contributions of Dr Yong-Ki Kim. As a consequence, we dedicate this report to his memory.

References

[1] Y.-K. Kim, http://physics.nist.gov/PhysRefData/Ionization/intro.html .

[2] H. Tanaka and M. Inokuti, The Special Volume "*Fundamentals of Plasma Chemistry*" *Adv. At. Mol. And Opt. Phys.* **43** (Academic Press, San Diego, 1999) 1-16.

[3] M. Itikawa, *Plasma Chemistry and Applications* (Springer-Verlag, 2007).

[4] R. J. Celotta and R. H. Huebner, *Electron Spectroscopy, Theory, Techniques and Ap-*

*plication*s, C. R. Brundle and A. D. Baker eds. (Academic Press, London, New York, San Francisco 1979) Vol. 3, 41-181.

[5] M. Inokuti, *Rev. Mod. Phys*. 43 (1971) 297.

[6] E. N. Lassettre, *J. Chem. Phys*. 43 (1965) 4479.

[7] Y.-K. Kim and M. E. Rudd, *Phys. Rev.* A 50 (1992) 3954.

[8] Y.-K. Kim, *Phys. Rev.* A 64 (2001) 032713.

[9] Y.-K. Kim, *J. Chem. Phys*. 126 (2007) 064305.

[10] H. Duetsch, K. Becker, M. Probst and T. D. Märk in *Adv. At. Mol. Opt. Phys*. 57, eds. P. R. Berman, E. Arimondo and C. C. Lin (Academic Press, Burlington, 2009) 87.

[11] M. Hoshino *et al*., *J. Phys*. B 42 (2009) 145202.

[12] H. Kato *et al*., *Phys. Rev*. A 77 (2008) 062708.

[13] H. Kato *et al*., *J. Chem. Phys*. 126 (2007) 064307.

[14] H. Kawahara *et al*., *Phys. Rev*. A 77 (2008) 012713.

[15] H. Kawahara *et al*., *J. Phys*. B 41 (2008) 085203.

[16] H. Kawahara *et al*., *J. Chem. Phys*. 131 (2009) 114307.

[17] P. A. Thorn *et a*l., *J. Chem. Phys*. 126 (2007) 064306.

[18] M. A. Khakoo *et al*., *Phys. Rev*. A 77 (2008) 102704.

[19] L. Vriens, *Phys. Rev*. 160 (1967) 100.

Please recall that more details on all the work presented in this report can be found in the original references cited above. In addition, our two previous NIFS Data reports:

M. Hoshino, H. Kato, C. Makochekanwa, S. J. Buckman, M. J. Brunger, H. Cho, M. Kimura, D. Kato, I. Murakami, T. Kato and H. Tanaka, 2008 "Elastic Differential Cross Sections for Electron Collisions with Polyatomic Molecules" (NIFS-DATA-101, Toki, Japan, ISSN 0915-6364), 1-60,

H. Kato, M. Hoshino, H. Kawahara, C. Makochekanwa, S. J. Buckman, M. J. Brunger, H. Cho, M. Kimura, D. Kato, H. A. Sakaue, I. Murakami, T. Kato and H. Tanaka, 2009 "Cross Sections for Electron-induced Resonant Vibrational Excitations in Polyatomic Molecules" (NIFS-DATA-105, Toki, Japan, ISSN 0915-6364), 1-51,

should also be consulted.